General Disclaimer

One or more of the Following Statements may affect this Document

- This document has been reproduced from the best copy furnished by the organizational source. It is being released in the interest of making available as much information as possible.

- This document may contain data, which exceeds the sheet parameters. It was furnished in this condition by the organizational source and is the best copy available.

- This document may contain tone-on-tone or color graphs, charts and/or pictures, which have been reproduced in black and white.

- This document is paginated as submitted by the original source.

- Portions of this document are not fully legible due to the historical nature of some of the material. However, it is the best reproduction available from the original submission.

JPL PUBLICATION 85-33

Microwave Properties of a Quiet Sea

J.M. Stacey

May 15, 1985

NASA
National Aeronautics and
Space Administration

Jet Propulsion Laboratory
California Institute of Technology
Pasadena, California

TECHNICAL REPORT STANDARD TITLE PAGE

1. Report No. JPL 85-33	2. Government Accession No.	3. Recipient's Catalog No.
4. Title and Subtitle Microwave Properties of a Quiet Sea		5. Report Date May 15, 1985 6. Performing Organization Code
7. Author(s) Joé Stacey		8. Performing Organization Report No.
9. Performing Organization Name and Address JET PROPULSION LABORATORY California Institute of Technology 4800 Oak Grove Drive Pasadena, California 91109		10. Work Unit No. 11. Contract or Grant No. NAS7-918 13. Type of Report and Period Covered JPL Publication
12. Sponsoring Agency Name and Address NATIONAL AERONAUTICS AND SPACE ADMINISTRATION Washington, D.C. 20546		14. Sponsoring Agency Code

15. Supplementary Notes

16. Abstract

The microwave flux responses of a quiet sea are observed at five microwave frequencies and with both horizontal and vertical polarizations at each frequency--a simultaneous 10-channel receiving system. The measurements are taken from Earth orbit with an articulating antenna.

The 10-channel responses are taken simultaneously since they share a common articulating collector with a multifrequency feed.

The plotted flux responses show: The effects of the relative, on-axis-gain of the collecting aperture for each frequency; The effects of polarization rotation in the output responses of the receive when the collecting aperture mechanically rotates about a feed that is fixed; The difference between the flux magnitudes for the horizontal and vertical channels, at each of the five frequencies, and for each pointing position, over a 44-degreee scan angle; The RMS value of the clutter--as reckoned over the interval of a full swath for each of the 10 channels. The clutter is derived from the standard error error of estimate of the plotted swath response for each channel.; The expected value of the background temperature is computed for each of the three quiet seas. The background temperature includes contributions from the cosmic background, the downwelling path, the sea surface, and the upwelling path.

The three quiet seas that are observed are: an area on the Equator in the Pacific; near South America; one at a mid-latitude in the Sargasso Sea; and one at a high latitude in the Indian Ocean, near Madagascar and Antarctica. Comparisons among the flux measurements of the three quiet seas are drawn and the results analyzed.

17. Key Words (Selected by Author(s))	18. Distribution Statement
Geosciences and Oceanography (General) Earth Resources Meteorology and Climatology Space Sciences (General)	Unlimited/Unclassified

19. Security Classif. (of this report)	20. Security Classif. (of this page)	21. No. of Pages	22. Price
Unclassified	Unclassified		

JPL PUBLICATION 85-33

Microwave Properties of a Quiet Sea

J.M. Stacey

May 15, 1985

National Aeronautics and
Space Administration

Jet Propulsion Laboratory
California Institute of Technology
Pasadena, California

The research described in this publication was carried out by the Jet Propulsion Laboratory, California Institute of Technology, under a contract with the National Aeronautics and Space Administration.

ABSTRACT

The microwave flux responses of a quiet sea are observed at five microwave frequencies and with both horizontal and vertical polarizations at each frequency--a simultaneous 10-channel receiving system. The measurements are taken from Earth orbit with an articulating antenna.

The 10-channel responses are taken simultaneously since they share a common articulating collector with a multifrequency feed.

The plotted flux responses show:

- The effects of the relative, on-axis-gain of the collecting aperture for each frequency.
- The effects of polarization rotation in the output responses of the receiver when the collecting aperture mechanically rotates about a feed that is fixed.
- The difference between the flux magnitudes for the horizontal and vertical channels, at each of the five frequencies, and for each pointing position, over a 44-degree scan angle.
- The RMS value of the clutter--as reckoned over the interval of a full swath for each of the 10 channels. The clutter is derived from the standard error of estimate of the plotted swath response for each channel.
- The expected value of the background temperature is computed for each of the three quiet seas. The background temperature includes contributions from the cosmic background, the downwelling path, the sea surface, and the upwelling path.

The three quiet seas that are observed are: an area on the Equator in the Pacific, near South America; one at a mid-latitude in the Sargasso Sea; and one at a high latitude in the Indian Ocean, near Madagascar and Antarctica. Comparisons among the flux measurements of the three quiet seas are drawn and the results are discussed and analyzed.

Observational problems arise from rotating a collecting aperture around the directional diagram of a fixed feed. Some of these problems are discussed, and one alternate solution is given.

ACKNOWLEDGEMENTS

The software development and computer programming skills of Stephen N. and Janis L. Kitzis made this monograph possible:

- They structured an interpolation program that brought all of the flux responses (digital counts) for all 10 channels of the microwave receiver into time coincidence with the vertical 37-GHz channel --for all pointing positions of the articulating collector.

- They retrieved the digital record of the orbiting microwave sensor from archive and keyed each pointing position of its collecting aperture, across a swath, to latitude and longitude coordinates.

- Then they organized the digital record so that all of the pointing positions of the articulating collecting aperture, as it moved across a swath, showed all of the needed information, i.e, digital counts (flux magnitude), collector scan angle, latitude, and longtitude.

With this kind of digital record to work with, writing this monograph was a trivial task.

The visible and infrared images of the cloud patterns over the three quiet seas were made available from:

- The USAF DMSP (Defense Meteorological Satellite Program). The film transparencies are archived for NOAA/NESDIS at the University of Colorado, CIRES/National Snow and Ice Data Center

and from

- NOAA/NESDIS, National Environmental Satellite Data, and Information Service.

TABLE OF CONTENTS

Tables

Figures

TABLE OF CONTENTS (Continued)

Figures

Exhibits

TABLE OF CONTENTS (Continued)

TABLE OF CONTENTS (Continued)

BACKGROUND

The surface of the sea covers a very large fraction of the surface of the Earth. For this reason alone it is not surprising that we seek to understand better the properties of the sea, on and below its surface.

One elegant way to observe the sea is by remote sensing of its surface with spaceborne sensors--particularly, those that operate in the visible, infrared, and microwave intervals of the spectrum.

Visible sensors, for example, are applied to investigate the roughness and color patterns of the sea's surface on the scale of a few micrometers. The presence of clouds, or water particulates of any kind in the atmosphere are catastrophic to the accuracy and the precision of visible wavelength measurements. In the visible region of the spectrum even fair-weather cumulus clouds are opaque.

Microwave wavelengths penetrate seawater to a depth of a few millimeters. By expectation, an 8-mm wavelength penetrates to a depth of 2 mm or less. The surface conductivity of seawater is high at microwave wavelengths (nominally, 4.5 mhos/meter) and it is this electrical quantity that controls the depth of penetration (skin depth). Microwave sensors measure the thermal properties of the sea's surface and they are unaffected by the occurrence of tenuous (cirrus) and moderately dense (fair-weather cumulus) cloudforms. Raining clouds, and cloudforms that contain particulate water, produce relatively high attenuation.

Microwave sensors possess some obvious and important advantages over visible and infrared sensors. Good cloud penetration has already been mentioned--the polarized properties of the sea is another. At microwave wavelengths the sea may be observed with multiple polarizations at each wavelength. From these polarized properties, differences and ratios may also be formed. The difference between the fluxes for the horizontal and vertical polarizations, for example, serves as a discriminant from which important sea properties may be inferred--e.g, sea roughness or the occurrence of pollutants, such as oil films.

QUIET SEA MEASUREMENTS

The flux emissions from three quiet seas are measured and reported by a microwave imager that operates in Earth orbit. The observing geometry is shown in Figures 1 and 2 [see Note (1)]. The measurements are taken at five different frequencies and with both horizontal and vertical polarizations at each frequency--a 10-channel imager.

A quiet sea denotes a sea state where the products of air-sea interactions (foam, bubbles, spray) are minimized, and connotes that the quiet sea serves as a reference level sea condition, for comparisons with other sea states, as it is observed from orbit with microwave sensors.

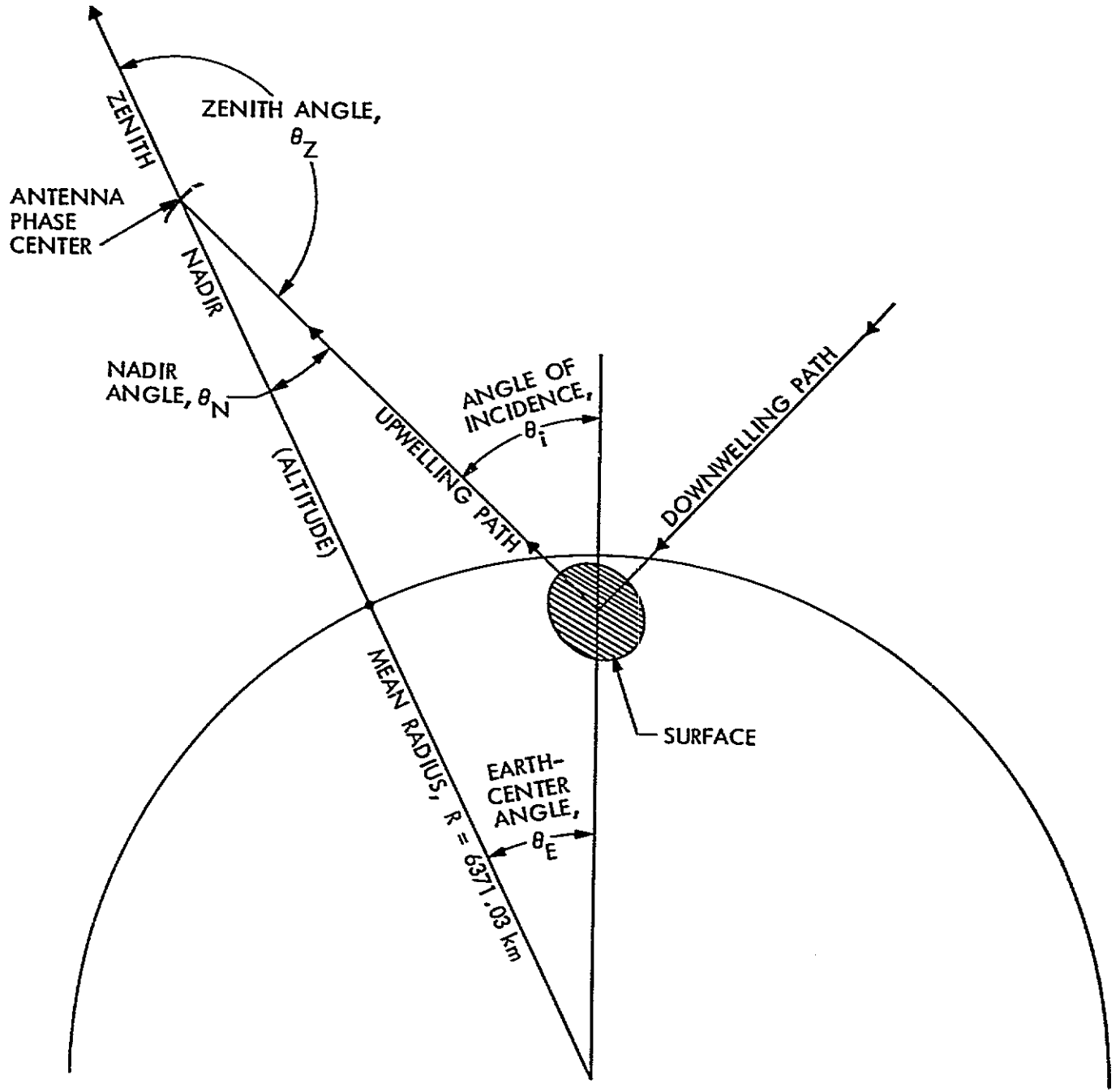

Figure 1. Geometrical Definitions

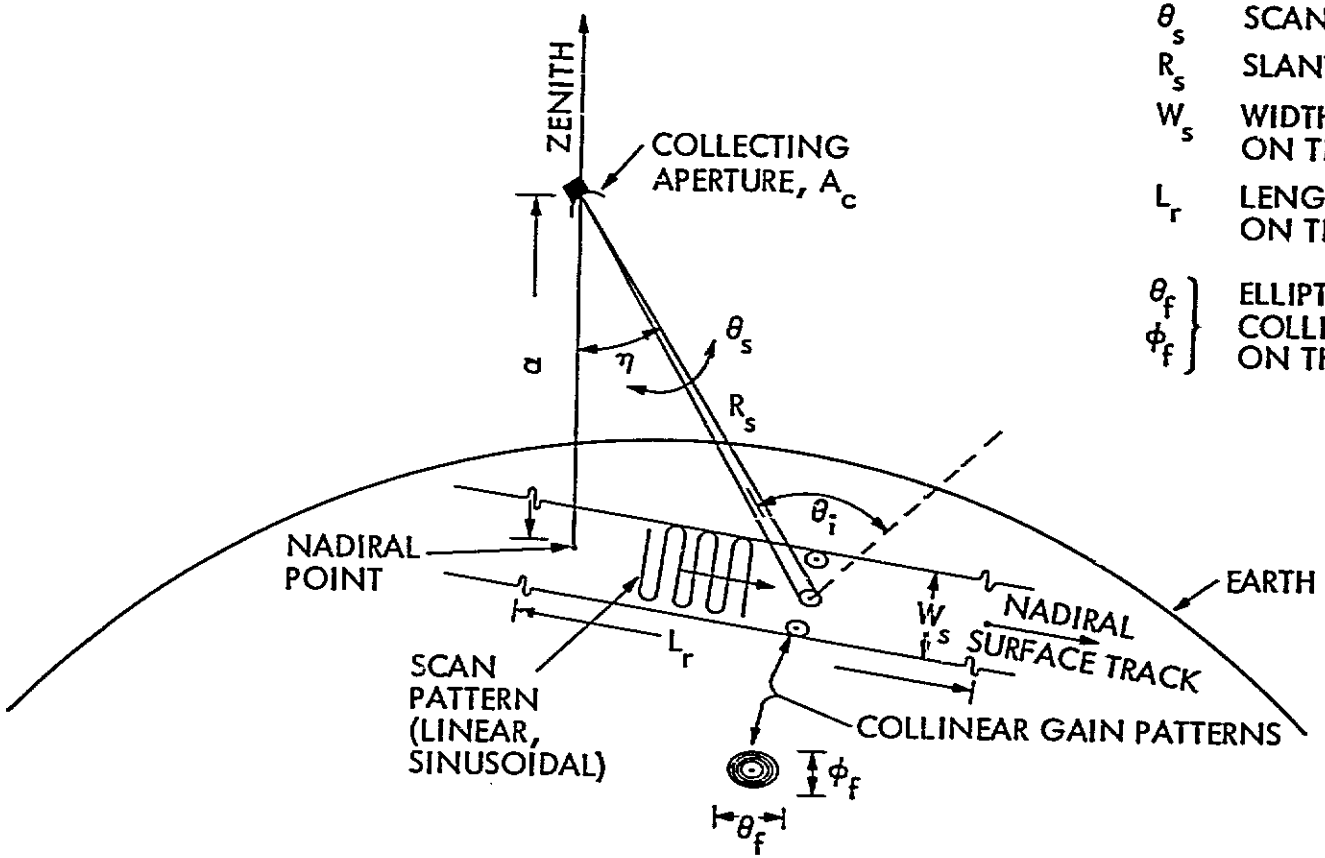

LEGEND

α	ALTITUDE
η	NADIRAL ANGLE
θ_i	INCIDENCE ANGLE
θ_s	SCAN ANGLE (CONSTANT θ_i)
R_s	SLANT RANGE
W_s	WIDTH OF SCANNED SEGMENT ON THE SURFACE
L_r	LENGTH OF SCANNED SEGMENT ON THE SURFACE
θ_f, ϕ_f	ELLIPTICAL PROJECTION OF COLLINEAR GAIN PATTERNS ON THE SURFACE

Figure 2. Sector Scan Geometry From Orbit

In these analyses, the quiet sea implies further that the character of the prevailing cloud cover has been determined by visible or infrared photographs, and that the flux emissions from the clouds are reasoned to be unimportant as they affect the measurements.

More, the status of the quiet sea is qualified, as such, by an inspection of its polarized output responses and by a calculation of the background temperature T_B [2]. This includes a separate accounting of the emission contributions from:

- The cosmic background.
- The downwelling path.
- The emission from the quiet sea surface.
- The upwelling path.

The key importance of the microwave measurements of the quiet sea, as they are discussed here, is that the measurements are taken simultaneously, with the same collecting aperture and with the same multifrequency feed assembly. From this, the relative flux responses for each of the 10 channels are determined and comparisons among the channel responses are effectually and easily drawn.

One of the objectives for measuring the flux emitted by the quiet sea is to plot and analyze the primitive responses for each receiver channel over the interval of one swath, for the three quiet seas. Another objective is to interpret the flux responses and to draw comparisons among the responses. The plotted data are given in sufficient detail to permit individual investigators to analyze the data for their own purposes or to construct comparisons with the investigations of others.

The quiet sea is observed by the microwave imager at three different places and latitudes:

- In the Sargasso Sea--a mid-latitude
- On the Equator in the Pacific, near South America.
- At a high latitude in the Indian Ocean, near Antarctica.

Only one scan (swath) is plotted and analyzed for each of the three quiet seas. One scan is all that is needed.

Multiple observations of the quiet sea, at different latitudes and in a variety of maritime environments are reasoned to enhance and strengthen the comparisons among the quiet sea measurements and to build confidence by redundancy. Moreover, multiple measurements of several quiet seas strengthen comparisons and more readily show consistencies (and inconsistencies) in the receiver outputs where they occur.

From the detailed plots for each of the 10 channels and for each of three quiet seas:

(1) The pattern and the character of the emitted flux for both the horizontal and vertical channels are shown as they are affected by the rotation of the collecting aperture with respect to the feed.

(2) The point-by-point magnitudes of the differences between the horizontal and vertical polarizations are determined and plotted.

(3) The pattern of the clutter profile is plotted and the expected value of the RMS clutter is calculated for each channel.

THE IMAGER

The antenna assembly consists of a collecting aperture (79-cm diameter, 0.49 m^2 area), a multifrequency feed, and an electromechanical scanning mechanism (Figure 3). The collecting aperture and the feed operate in an offset, prime-focus configuration where the collector rotates with respect to the feed.

Allowing the collecting aperture to physically rotate with respect to the feed causes a continually changing orientation of both the horizontal and vertical vectors with respect to the plane of incidence at the sea surface. The incidence angle θ_i is maintained constant as the collector rotates.

The rotation of the horizontal and vertical vectors at the sea surface, as a function of the scan angle, is sometimes regarded to be a disadvantage because it produces an apparent distortion in the flux amplitudes that are returned by the sea.

Software processes are sometimes applied to remove the effects of polarization rotation from the primitive data. The antenna components may also be configured to maintain a fixed vector relationship while scanning, as will be shown later.

The principal advantage of rotating the collecting aperture with respect to the feed is that only the mass of the collector structure itself is rotated. Because of this, great economies are realized in the manufacture of the instrument, and in its implementation on the spacecraft.

If system design specifications require that the horizontal and vertical vector relationships remain constant during the observations of the sea surface (that is, if the vertical vector must remain fixed in the plane of incidence and the horizontal vector must remain fixed in the plane of the sea surface) for any scan angle, then the collector and the feed must maintain a fixed mechanical relationship--one with respect to the other, at all times. (See Figure 4.)

One concept for maintaining a fixed mechanical relationship between the collector and the feed (no relative motion) is illustrated in Figure 5, using the same antenna components as illustrated in Figure 3.

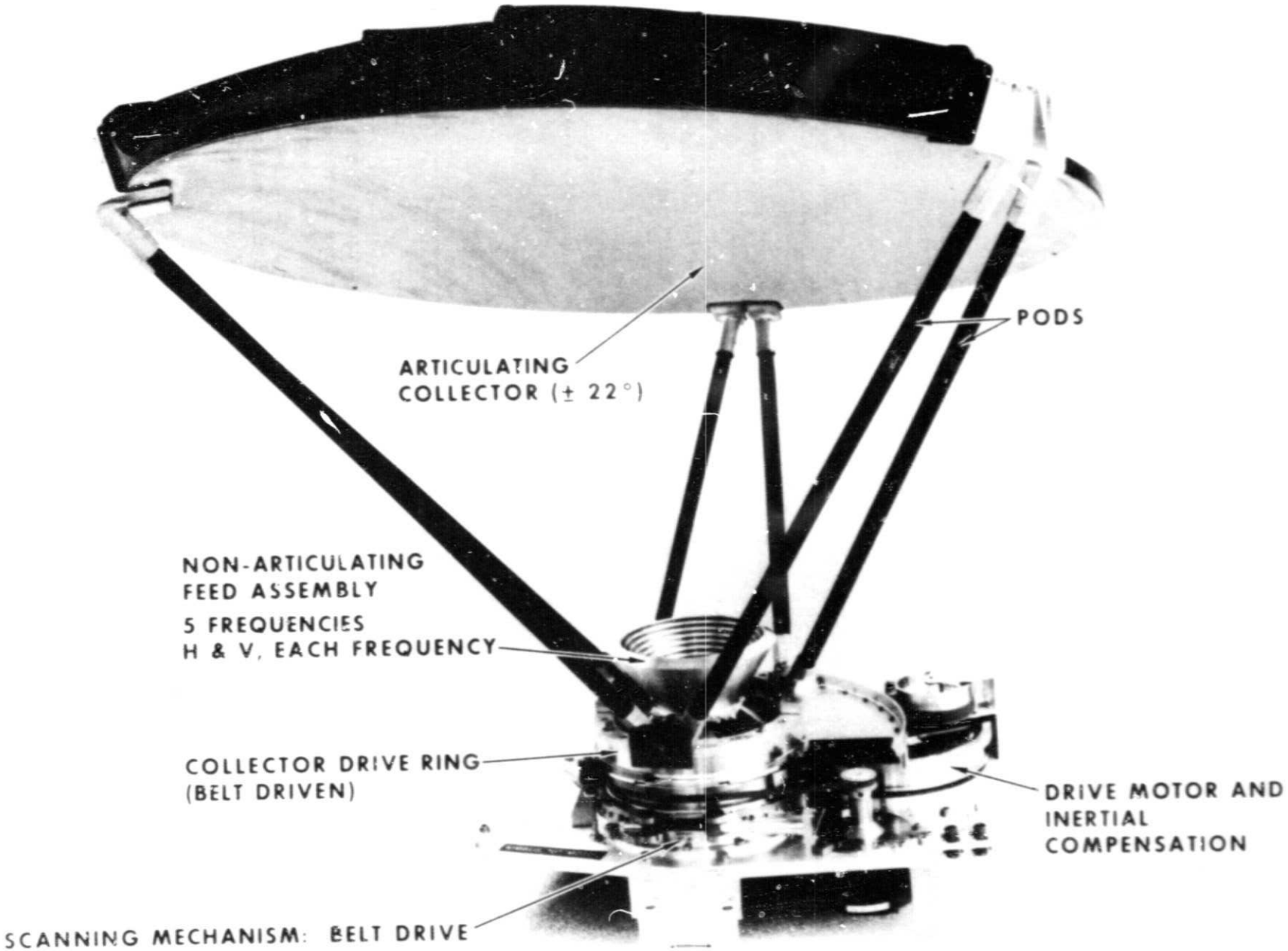

Figure 3. Articulating Collector and Scanning Mechanism

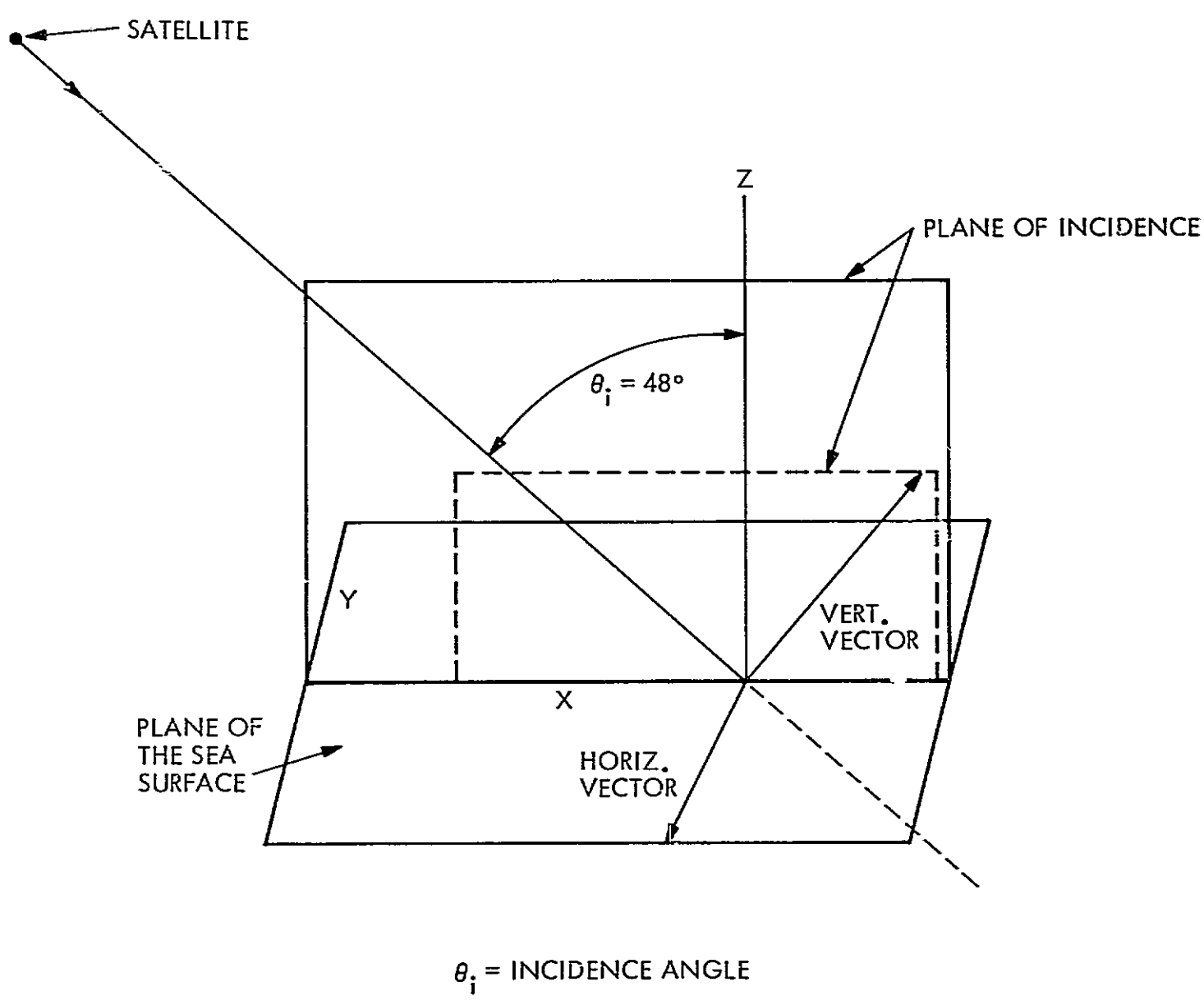

θ_i = INCIDENCE ANGLE

Figure 4. Polarization Relationships at the Sea Surface

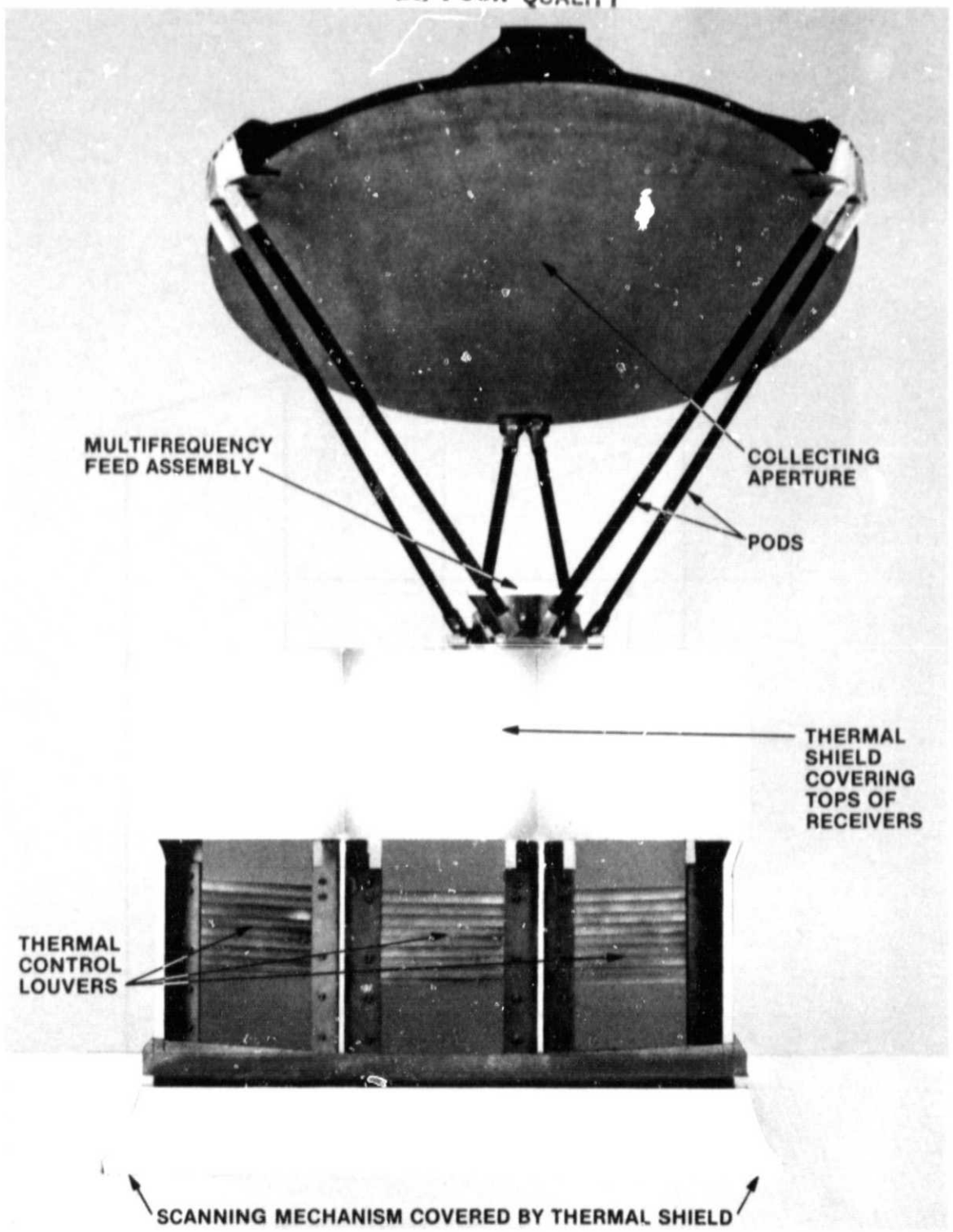

Figure 5. Concept of a Sector Scanning Instrument Where the Collecting Aperture and the Feed Maintain a Fixed Geometrical Relationship. (The entire instrument is rotated in a sector scan pattern by the scanning mechanism in the base.)

In Figure 5, the collector is rigidly and mechanically secured to the feed structure--there is no relative rotation of any kind. Notably, the entire instrument is rotated as a single, integral assembly: the collector, the feed, and the receivers, including the thermal shields and cooling devices. The scanning mechanism supports the entire mass of the instrument and provides for its rotation as a single mechanical assembly.

MORE ON POLARIZATION

The orbital geometry that affects the relative projections of the horizontal and vertical vectors on the sea surface is displayed in Figure 1.

Consider a spacecraft antenna whose pointing axis is directed at the nadiral point on the Earth. Consider further that the antenna is linearly polarized in its horizontal and vertical vectors. For the nadiral case, the flux density of the wavefront that arrives at the collecting aperture is equal for both horizontal and vertical polarizations, and the information content in their respective microwave responses is ambiguous. As the nadiral angle increases, the flux relationships change between the two polarizations--the difference in their flux intensities increases and the information content in their outputs decorrelates.

OBSERVED PROPERTIES OF QUIET SEAS

The microwave properties of three quiet seas are measured, plotted, and analyzed in Exhibits 1, 2, and 3. We chose the Sargasso Sea, the Equator area (west of Equador, South America), and the Indian Ocean, near Madagascar and Antarctica. These quiet seas were selected as candidates after an abundance of such seas were investigated. Many candidate seas were rejected because of the prevalence of high sea states, or because of poor weather with dense cloudforms.

It is useful to compare the properties of more than one quiet sea--especially, the polarization properties. A plurality of sea measurements of the same kind instills confidence from the comparisons and contributes robustness in reporting the results.

For each of the quiet seas investigated, the cloud cover is determined from visible and infrared photographs. The location of the center of the scanned swath is identified, in some way, on the photographs. The cloud-cover photos are taken in close time coincidence (a few hours--more or less) with the time of the observations.

The cloud-cover photos convey convincing evidence of the prevailing cloud conditions during the time of the passive microwave measurements of the quiet seas.

It is convenient for exacting comparisons among the seas that the Sargasso Sea and the Equator area measurements appear to be strikingly similar. That is, they possess low wind speeds and the character of their cloud cover is not

significantly different. Per contra, the Indian Ocean is considerably more cloudy. Because of the apparent differences in the cloud cover among the quiet seas, the effects of clouds are more easily perceived in the primitive data.

It is known, that when sea states are high, the flux from the sea increases in both the horizontal and vertical channels. The output responses of the vertical and horizontal channels increase together as the sea state increases --they merge to a common flux level to the point where the difference between them is small and sometimes the separation is barely distinguishable.

For a truly quiet sea condition, and when the angle of incidence is constant, there is an important and noticeable numerical difference between the flux levels for the horizontal and vertical channels, at all frequencies. That is, a large separation between the flux levels (digital counts) for the vertical and horizontal channels truly characterizes a quiet sea. Clear manifestations of a large separation between the horizontal and vertical channels for each frequency were imposed as a criterion in the selection of the quiet sea areas for this monograph.

The difference in the flux intensities between the horizontal and vertical channels is also a function of the roughness of the sea surface on the scale of the observing wavelength. For example, when the sea is rough on the scale of 8 mm, the 37-GHz (8-mm wavelength) polarized channels will tend to converge and exhibit smaller differences in the flux intensities between them. Under the same conditions, a scale of roughness of 8-mm is insignificant when viewed at an operating frequency of 6.6 GHz (4.6-cm wavelength)--and a large separation is steadfastly maintained between the horizontal and vertical channels.

THE PRIMITIVE RESPONSES

The relative flux responses for the quiet seas are expressed by the primitive responses of the receiver channels. No attempt is made to process or modify the primitive data that has been collected, in any way. The primitive responses are reported in relative digital counts. Digital counts are dimensionless units proportional to relative volts, or amperes, that are impressed across a common output resistance. In this basic sense, digital counts may be reckoned as relative watts that are proportional to the power density of the waveform appearing at the collecting aperture.

GAIN SCALE FACTOR

The gain scale factor is determined, before launch, while in the laboratory by the methods described in [1]. The gain scale factor for all channels is 8 (digital counts)/K for all 10 channels. From the gain scale factor, conversions from digital counts to equivalent thermodynamic temperatures can be conveniently and approximately made provided that the differences in the digital counts are small.

For example, the difference between the flux levels that exists between the horizontal and vertical channels, or the clutter that is expressed by its RMS value or standard error of estimate, may be converted into equivalent thermodynamic temperatures by the gain scale factor, insofar as all are properly regarded as approximations.

ANTENNA GAIN CONSIDERATIONS

The investigator is informed that the proper interpretation of the analyses and plots of the quiet seas, as they are displayed in Exhibits 1, 2, and 3, are importantly and significantly influenced by the antenna gain function [see Note (2)] for each operating frequency.

The magnitude of the digital counts for any frequency of operation is directly proportional to the antenna gain. For example, using Exhibit 1, the Sargasso Sea, the magnitude of the digital counts for the horizontal and vertical channels at 37 GHz are numerically higher than the digital counts for the corresponding horizontal and vertical channels at 21 GHz . . . and so on down to the lowest operating frequency at 6.6 GHz. This is a reasonable expectation because it is known--both theoretically, and by experience--that the spatial transfer of microwave power is based directly on antenna gain [2].

It is relevant to consider that the gain scale factor (a slope) is determined in the laboratory. Further, the gain scale factor is computed from the output responses of the receiver channels as the multifrequency-feed aperture views a variable-temperature blackbody load. From this procedure, it is clear, that the output digital counts are not influenced by the antenna gain until the instrument arrives in orbit when the collector is, for the first time, properly illuminated by the feed.

The plotted data in Figure 6 portray the expected proportionality of digital counts versus antenna gain for the vertical channels (an arbitrary selection) at the five frequencies. The digital counts are plotted for the vertical channels (an arbitrary choice) for each of the five frequencies, and at the center of the scan ($\theta_s = 0$) for each of the three quiet seas. The plotted data in Figure 6 are taken from the summary of the three quiet seas as given in Table 1. From Table 1, the quantity D_o is plotted for all of the vertical channels.

The key consideration shown in Figure 6 is that the digital counts, taken at the center of the scan, for all of the vertical channels, increase in magnitude in direct proportion to the antenna gain. On the log-log plot, there is a straight-line relationship between the measured digital counts and the computed antenna gain. By expectation then, the magnitude of the output responses of the receiver channels will vary directly with frequency or inversely with the operating wavelength as it is expressed in Note (2).

In Figure 6, the plotted points that relate antenna gain to digital counts for the Sargasso Sea and for the Equator are nearly identical--in fact, as a practicality, they superpose. For this reason, only one common line is plotted.

Table 1. Summary of the Primitive Responses of Three Quiet Seas

	SARGASSO				EQUATOR				INDIAN OCEAN			
POL/ GHz	D_0 (COUNTS)	δ (COUNTS)	G_0 (dB)	R(V, H)	D_0 (COUNTS)	δ (COUNTS)	G_0 (dB)	R(V, H)	D_0 (COUNTS)	δ (COUNTS)	G_0 (dB)	R(V, H)
V37	2466	14.75	49.26	-0.45	2455	10.97	49.26	0.02	2365	10.70	49.26	-0.41
H37	2165	14.87	49.26		2185	9.64	49.26		2040	8.73	49.26	
D37	301	-	-		270	-	-		325	-	-	
V21	2405	8.74	44.33	0.10	2398	5.39	44.33	0.03	2110	3.27	44.33	0.40
H21	2145	14.87	44.33		2153	4.88	44.33		1760	4.33	44.33	
D21	260	-	-		245	-	-		350	-	-	
V18	2240	5.80	42.98	-0.83	2229	6.09	42.98	-0.66	2130	4.21	42.98	-0.42
H18	1840	7.05	42.98		1855	4.47	42.98		1706	4.41	42.98	
D18	400	-	-		374	-	-		424	-	-	
V10	2105	3.50	38.46	-0.97	2105	4.96	38.46	-0.79	2023	3.50	38.46	-0.90
H10	1680	3.84	38.46		1702	3.88	38.46		1639	5.18	38.46	
D10	425	-	-		403	-	-		384	-	-	
V6	2015	3.77	34.33	-0.91	2008	2.53	34.33	-0.68	1915	2.27	34.33	-0.95
H6	1620	6.06	34.33		1640	2.02	34.33		1580	4.16	34.33	
D6	395	-	-		368	-	-		435	-	-	

LEGEND

θ_s ANTENNA SCAN ANGLE IN DEGREES

θ_0 CENTER OF SCAN, $\theta_s = 0$

D_0 DIGITAL COUNTS, RECEIVER OUTPUT, AT θ_0

δ STANDARD ERROR OF ESTIMATE, POLYNOMIAL FIT, $\theta_s = 44$, DIGITAL COUNTS.

→ EXPECTED VALUE FOR THE CLUTTER MAGNITUDE

G_0 GAIN OF THE COLLECTING APERTURE, dB

R(V, H) CORRELATION COEFFICIENT BETWEEN V AND H RECEIVER CHANNELS FOR $\theta_s = 44$

GSF GAIN SCALE FACTOR = 8 DIGITAL-COUNTS/KELVIN

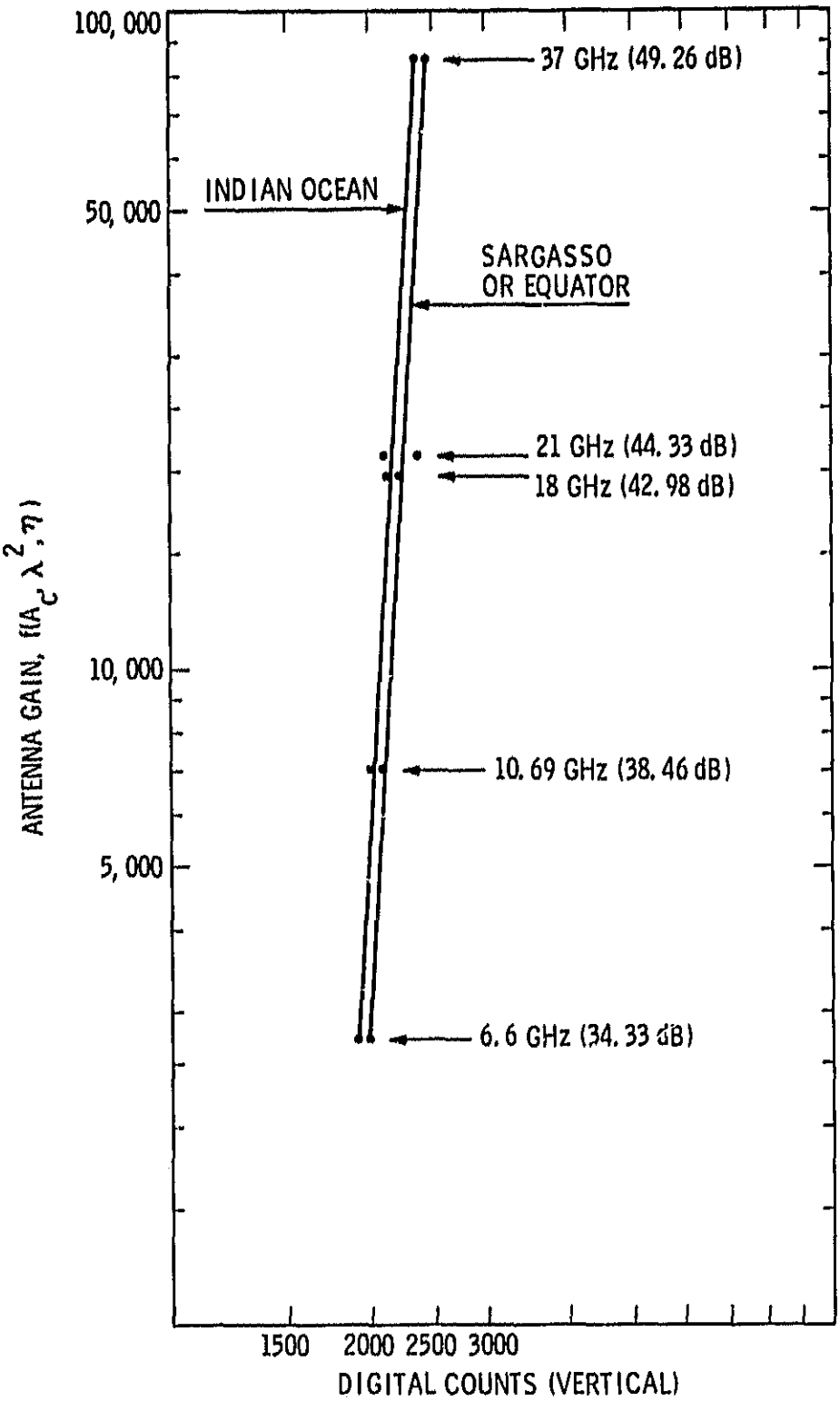

Figure 6. Digital Counts Versus Antenna Gain

Except at 21 GHz, the plotted points for all frequencies superpose on the regression line. In the plots, the 21-GHz responses are ignored, by choice, because the output responses are capriciously and significantly affected by atmospheric water vapor--because of this, they are regarded as aberrations.

In Figure 6, the same type of plot is shown for the Indian Ocean. Again the plotted points superpose on the straight regression line--except for the point at 21 GHz. The regression line shows a systematic offset to the left, which conforms with the expectation, because of higher cloud attenuation experienced in the propagation path at this quiet sea site.

The antenna gain for all frequencies is indicated on the plot where it is seen that the gain ranges from 34.33 dB at 6.6 GHz to 49.26 dB at 37 GHz--a spread of nearly 15 dB. This wide range in antenna gain is of considerable importance because it affects the manner in which surface features are detected and displayed. It is also important to realize that at 37 GHz there are 97 wavelengths across the diameter of the 79-cm collecting aperture--and at 6.6 GHz, there are only 17. The fewer number of wavelengths appearing across the collecting aperture at 6.6 GHz portends that the efficiency of the collecting aperture is much lower than 37 GHz.

Again, we are reminded that the plotted data in Figure 6 clearly show that the output responses for each channel (digital counts) are a well defined and linear function of the antenna gain.

Also in Figure 6, the plotted points and the regression line for the Indian Ocean appear to be displaced slightly to the left of the regression line for the Sargasso Sea and the Equator area. The reason for the displacement is because the cloud cover for this quiet sea produces higher attenuation than for the others.

QUIET SEA COMPARISONS

The measured data, taken by the microwave sensor on the SEASAT spacecraft, for the three quiet seas, are plotted and described in Exhibits 1, 2, and 3. The results of these measurements are summarized in Table 1.

Table 1 tabulates for each of the quiet seas:

- The digital counts measured at the center of the swath D_0 for each of the 10 channels, and the influence on them by the antenna gains at each frequency. These data are plotted in Figure 6 for the vertical channels for the three quiet seas. Also tabulated are the differences between the horizontal and vertical polarizations at each frequency.

- The standard error of estimate (SEE) of the clutter variations computed over the swath. The SEE operates as the expected value for the RMS clutter as it is computed across the interval of a swath [see Note (4)].

- The antenna gain (dB) for each frequency

- The correlation coefficient, R, expresses the fraction of the variations in the horizontal channel that are explained by the variations in the vertical channel [see Note (3)].

It is interesting and relevant to discuss some comparisons between the Sargasso Sea and the Equator in Table 1.

The digital counts, D_o, for the vertical channels for the Sargasso Sea and for the Equator, for example, progressively decrease in magnitude from the V37 channel down to the V6 channel, i.e.:

	SARGASSO	EQUATOR
V37	2466	2455
V21	2405	2398
V18	2240	2229
V10	2105	2105
V6	2015	2008

which is consistent with their proportionality to antenna gain. The absolute values of the digital counts are also remarkably similar--the differences between the absolute values are only a few percentage points. In fact the differences are less than 0.5%--which can be interpreted to mean that the two quiet seas were observed under remarkably similar conditions.

Also note that the differences in the digital counts between the horizontal and vertical channels, e.g., D37, D21, D18 . . ., are approximately the same magnitudes--by expectation they are influenced by the same statistics. The differences between the digital counts for the vertical and horizontal channels, D37 for example, are 301 and 270, respectively. From the gain scale factor, these differences translate into an equivalent thermodynamic temperature difference of 301/8 = 38 K and 270/8 = 34 K at the centers of the swath.

The RMS clutter does not seem to bear any particular consistency with anything except that the clutter decreases in magnitude at the lower frequencies--which is consistent with lower antenna gain. The lower antenna gain causes the receiver channels to be less sensitive to the detection of surface features such as surface roughness and thermal gradients. Also, clutter components arriving in the sidelobes are reduced [Note (4)]. The standard error of estimates for the V37 and H37 channels are 14.75 and 10.97 digital counts, respectively. From the gain scale factor, the RMS clutter is transformed into equivalent thermodynamic temperatures by 14.75/8 = 1.8 K and 10.97/8 = 1.4 K, respectively.

It is of critical significance to realize that the estimates for RMS clutter magnitudes are the expected values for the clutter as it is determined over the extent of an entire swath. The procedure for calculating the clutter (standard error of estimate) magnitude is determined by a best-fit polynomial

to the 47 pointing positions of the collector that occur across a swath. Typically, the Exhibits show the order of the polynomial that was used to determine the magnitude of the standard error of estimate across the swath. Mostly, the SEE tends to overestimate the magnitude of the clutter.

Where emitting objects occur on the surface of the quiet sea; such as currents, warm and cold eddies, pollutants, wide-scale debris, etc., the clutter is computed across the swath in the immediate vicinity (local scan angle) of the emitting object. When the clutter is computed in this manner it is treated as a local clutter element and it may, in fact, occur that the local clutter, as it is computed, may be considerably different than the expected value.

THERMODYNAMIC TRANSFER OF TEMPERATURE FROM THE BACKGROUND

The phase center of the antenna views the thermodynamic temperature of the background (and its temperature changes) as the articulating collector scans a 44-degree sector on the Earth--see Figure 2.

The background temperature, T_B, consists of 4 path-segments (terms) as shown in Figure 7--namely, the temperature contributions from: the cosmic background, the downwelling path, the emitted surface temperature, and the upwelling path [2]. The terms of T_B are defined in Figure 7.

Each of the quiet seas (Exhibits 1, 2, and 3) contains an estimate of T_B, at an operating wavelength of 8-mm.

Exhibits 1 and 2 give an estimate for T_B for clear weather conditions as shown in Figures E1-3 and E2-3, respectively.

Exhibit 3 (Indian Ocean) gives an estimate for T_B (Fig. E3-3) for a stratus cloud condition whose density is 0.2 grams/m^2. For the Indian Ocean, a cloud attenuation factor of 0.163 dB is introduced into both the downwelling and the upwelling paths. The cloud emission summary is shown in Table E3-1.

DETECTION CRITERIA

The plotted responses for the horizontal and vertical channels and for the three quiet seas (Exhibits 1, 2, and 3) show evidence of the occurrence of surface features, such as warm and cold currents and small eddies. Currents and eddies are manifested as temperature gradients which equivalently transform into flux variations.

The signatures of many surface features are apparent in the plots of the horizontal and vertical channels at 37 GHz. By comparison, the manifestations of surface features diminish significantly at lower frequencies. The relatively high antenna gain at 37 GHz explains its superiority in the detection of surface features.

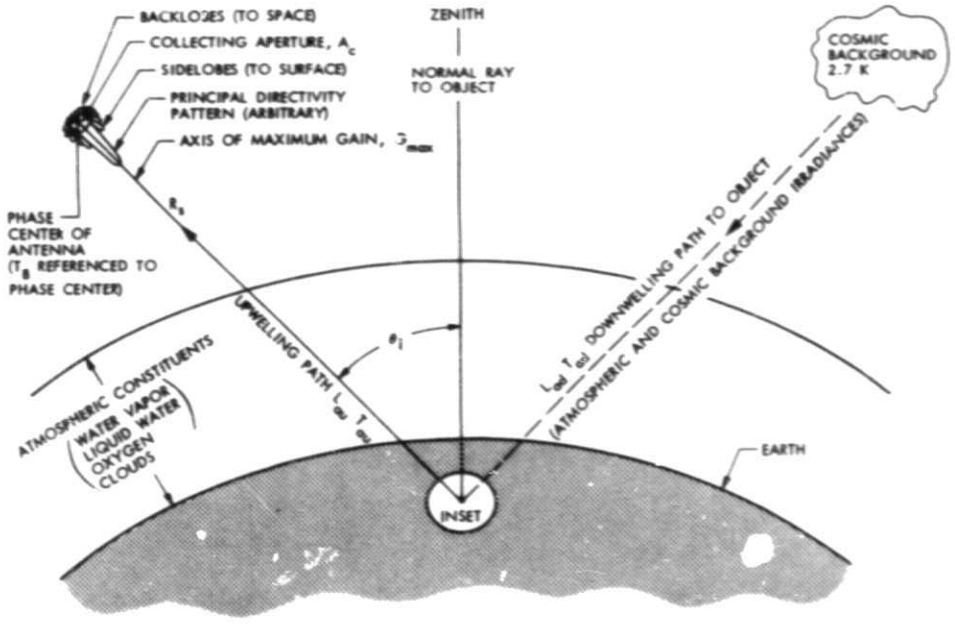

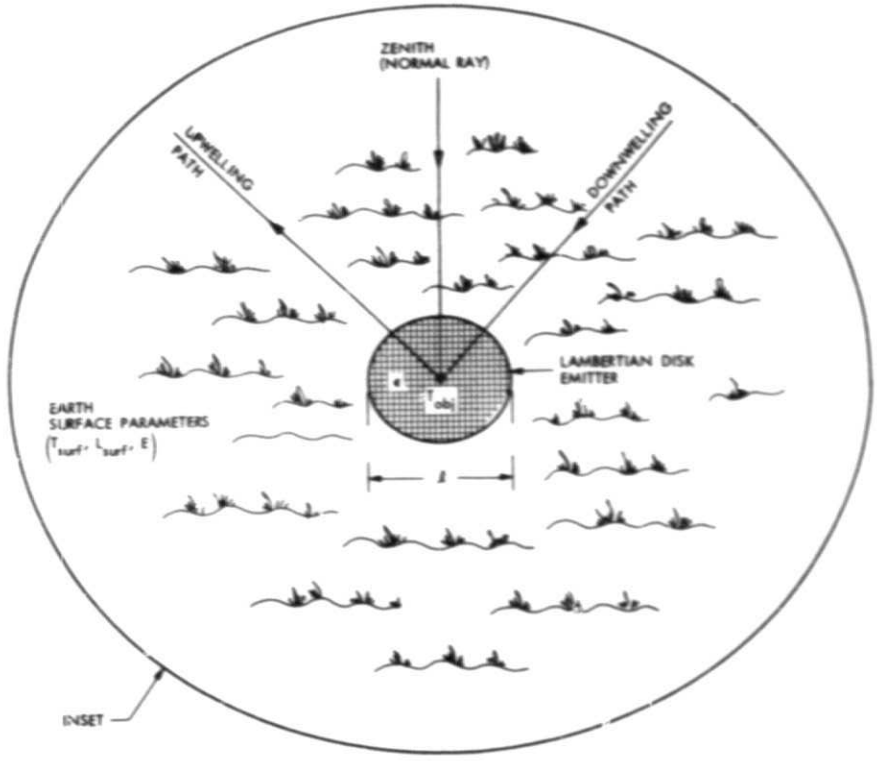

LEGEND

T_{au} = INTEGRATED PHYSICAL TEMPERATURE OF THE UPWELLING PATH, K

L_{au} = LOSS IN THE UPWELLING PATH

T_{surf} = PHYSICAL TEMPERATURE OF THE SURFACE MATERIAL, K

L_{surf} = LOSS IN THE SURFACE MATERIAL

T_{ad} = INTEGRATED PHYSICAL TEMPERATURE OF THE DOWNWELLING PATH, K

L_{ad} = LOSS DOWNWELLING PATH, K

T_B = THERMODYNAMIC TEMPERATURE OF THE BACKGROUND, K

T_{obj} = TEMPERATURE OF OBJECT (UNIFORM), K

ϵ = EMISSIVITY OF OBJECT

ℓ = DIAMETER OF OBJECT, m

R_s = SLANT RANGE (COLLECTING APERTURE TO OBJECT), m

A_c = AREA OF COLLECTING APERTURE, m^2

G_{max} = AXIS OF MAXIMUM ANTENNA GAIN

θ_i = INCIDENCE ANGLE, deg

$$T_B = \frac{T_{cosmic}}{L_{ad}\,L_{surf}\,L_{au}} + \frac{T_{ad}\,(L_{ad}-1)}{L_{ad}\,L_{surf}\,L_{au}} + \frac{T_{surf}\,(L_{surf}-1)}{L_{surf}\,L_{au}} + \frac{T_{au}\,(L_{au}-1)}{L_{au}}, \text{ K}$$

$\{$COSMIC$\}$ $[$DOWNWELLING$]$ $[$SURFACE$]$ $[$UPWELLING$]$

WHERE: ϵ = EMISSIVITY

$$L_{surf} = \frac{1}{1-\epsilon}$$

SUBSCRIPTED L SYMBOLS ARE DISSIPATIVE LOSSES EXPRESSED AS A NUMBER > 1.

Figure 7. Model for Computing the Thermodynamic Temperature of the Background

The detectivity of an emitting object on the surface of the Earth, as viewed by an orbiting receiver, is determined mainly by the area of the object and its temperature difference with respect to the background temperature T_B. From its areal extent, and its temperature difference with respect to T_B, the signal-to-clutter (S/C) ratio of the object may be computed as referenced to the phase center of the observing spaceborne antenna. For this computation, we refer to the expression for the transfer of microwave power from emitting objects on the surface to a collecting aperture in Earth orbit [2].

From [2, equation (11s)], the expression for S/C (Figure 8) is recast to solve for the diameter, ℓ, of the Lambertian Disk Emitter. From this recast expression, we compute the diameter of the disk, ℓ, that the antenna system can resolve.

Recasting the expression in Figure 8 to solve for ℓ,

$$\ell = \left[\frac{R_s^2 \, T' \, B \, L_{au} \, (S/C)}{2.57 \times 10^{14} \, \varepsilon \cos \theta_i \, T^4 \, (A_c \, \eta)} \right]^{1/2} , \text{ m} \qquad (1)$$

where

R_s = 1122 km

T' = 1.34 K (Taken as the expected value for the clutter, V37 channel, Exhibit 2, Equator quiet sea.)

B = 100 MHz

L_{au} = 0.35 dB (1.08)

(S/C) = 10 dB

ε = 0.35

θ_i = 48.77

T = 2.0 K

A_c = 0.49 m (0.79 m, circular diameter)

η = 0.9

From the estimates given in (1), ℓ = 2087 m.

The term ℓ expresses the diameter of the modeled disk (e.g., an eddy) that is detectable by the orbiting collector--given the assumptions for the terms in [2]. A further assumption is that the orbiting antenna operates efficiently as it extracts the signal power from the arriving wavefront.

$$(S/N) = \frac{\pi \sigma \epsilon \cos \theta_i T^4 \ell^2 (A_c \eta)}{4\left(4\pi R_S^2\right) L_{au} k T' B}, \quad \text{DIMENSIONLESS} \qquad (11a)$$

$$(S/N) = \frac{2.57 \times 10^{14} \epsilon \cos \theta_i T^4 \ell^2 (A_c \eta)}{R_S^2 T' B L_{au}}$$

WHERE

σ = 5.67032E+08 STEFAN-BOLTZMANN CONSTANT.

ϵ = EMISSIVITY OF EMITTING OBJECT (NORMAL INCIDENCE).

θ_i = ANGLE OF INCIDENCE, DEG.

T = DIFFERENCE TEMPERATURE: EMITTING OBJECT TEMPERATURE MINUS THE BACKGROUND TEMPERATURE $|T_{obj} - T_B|$, K

ℓ = DIAMETER OF EMITTING OBJECT, m

A_c = AREA OF COLLECTING APERTURE, m^2

η = SOLID ANGLE MAIN BEAM EFFICIENCY.

R_S = SLANT RANGE, m

L_{au} = ATMOSPHERIC ATTENUATION, A NUMBER > 1.0.

k = 1.380662E-23 BOLTZMANN CONSTANT.

T' = CLUTTER PLUS RECEIVER NOISE, ORTHOGONAL AVERAGE, K

B = PREDETECTION BANDWIDTH, HERTZ

Figure 8. Summary of the Power Transfer Equations (Surface to Orbit)

The plotted data shown in Exhibit 2 (Equator) for the V37 channel was taken by an articulating collector, in Earth orbit, operating at 8-mm wavelength. The on-axis gain of the collector is given in Figure 6 (49.4 dB)--98 wavelengths dispose across its 0.79-meter diameter.

AIR-SEA INTERACTIONS

It ought to be a simple thing to measure, with good accuracy, microwave flux intensities and flux variation that are radiated from a quiet sea. But it is not. The problems are legion.

First, we must deal with the uncertainties in the flux variations as they are corrupted by the emission from a capricious atmosphere in both the upwelling and the downwelling paths. Clouds, water particulates, water vapor, and oxygen all participate by their emissions to vitiate the measurements of the flux from a quiet sea.

Then there are the uncertainties in the reflectivity and the emissivity factors of the quiet sea itself as these factors are affected, in a matter of degree, by variable surface roughness--small as it may be.

More, the variations in the reflectivity cause other errors to propagate. For example, the flux emissions from the cosmic background and from the downwelling atmosphere vary their intensities as they arrive at the collecting aperture because of variable surface reflectivity. See Figure 8. Surface roughness and emissivity are known to be imponderables.

Even more serious factors arise. Microwave wavelengths penetrate the quiet sea to a depth of only a few millimeters. At 8-mm wavelength (37 GHz), the penetration depth (skin depth) is less than 2 millimeters; at a wavelength of 4.5 cm (6.6 GHz), the penetration depth is less than 3 mm. See Table 2.

The surface conductivity of seawater (4.5 mhos/meter) controls the depth of penetration. Typically, conductivity increases with thermometric temperature.

The dynamic motion of the quiet sea surface itself causes problems in the measurement of the liquid seawater.

The sea is in constant motion--and even on the quietest sea surface there are manifestations of foam and bubbles within the first few millimeters of its surface. Foam and bubbles are structured as spheres. The air volume within the sphere dominates the volume and, by expectation, importantly affects the thermometric temperature of the seawater on the surface of the sphere.

The importance of the matter is that the temperature of the air within the bubble or foam critically affects the flux radiation from the sea surface within the skin depth of a few millimeters.

Table 2. Penetration Depth (Skin Depth), cm

FREQUENCY (GHz)	AGRICULTURAL SENSE			DRY LIMESTONE	DRY SANDSTONE	ROCK SALT	MARINE SAND	CONNATE WATER (IN ROCKS)	ARIZONA SOIL	AUSTIN, TEXAS SOIL (VERY DRY)
	GOOD SOIL	AVERAGE SOIL	POOR SOIL							
6.633	2.6	8.3	26.4	87.4	61.8	87.4	0.83	0.87	1.95	7.18
10.69	2.0	6.6	20.8	68.8	48.7	68.8	0.66	0.69	1.54	5.66
18.0	1.6	5.1	16.0	53.1	37.5	53.1	0.51	0.53	1.19	4.36
21.0	1.5	4.7	14.8	49.1	34.7	49.1	0.47	0.49	1.10	4.04
37.0	1.1	3.5	11.2	37.0	26.2	37.0	0.35	0.37	0.83	3.04

FREQUENCY (GHz)	GLACIER ICE	FRESH-WATER ICE	SEA ICE	PERMAFROST	SNOW (DRIFTED, WET)	SEAWATER	FRESH WATER
6.633	663	195	21.4	87.3	113	0.29	26.4
10.69	487	154	16.9	68.8	88.9	0.23	20.8
18.0	375	119	13.0	53.1	68.5	0.18	16.0
21.0	347	110	12.0	49.1	63.4	0.16	14.8
37.0	262	83	9.1	37.0	47.8	0.12	11.2

NOMINAL VALUES OF SURFACE CONDUCTIVITY IN MHOS/METER*

• GOOD SOIL	0.055	• GLACIER ICE	1E-06
• AVERAGE SOIL	0.0055	• FRESH-WATER ICE	1E-05
• POOR SOIL	0.00055	• SEA ICE (-40 C)	8.33E-04
• DRY LIMESTONE	5E-05	• PERMAFROST	5E-05
• DRY SANDSTONE	1E-04	• SNOW (DRIFTED, WET)	3E-05
• ROCK SALT	5E-05	• SEAWATER	4.5
• MARINE SAND	0.55	• FRESH WATER	5.5E-04
• (CONNATE WATER IN ROCKS)	0.5		
• ARIZONA SOIL	0.1		
• AUSTIN, TEXAS SOIL (DRY)	0.0074		

*SURFACE CONDUCTIVITY VARIES WIDELY WITH FREQUENCY, TEMPERATURE, WATER CONTENT, IMPURITIES,... AND OTHER FACTORS. THE VALUES GIVEN FOR SURFACE CONDUCTIVITY ARE ADOPTED FOR PLANNING PURPOSES OR FOR GENERAL INTEREST. MAINLY, THEY ARE BASED ON LOW-FREQUENCY MEASUREMENTS <100 KHz, OR ARE DERIVED FROM CASUAL EXTRAPOLATIONS AT MICROWAVE WAVELENGTHS.

It is known that the air temperature and the liquid seawater temperature in the air-sea interaction zone can be different by many degrees--at high latitudes by even tens of degrees. When the air is encapsulated by the spherical walls of seawater (foam and bubbles), the air affects the temperature of the seawater in the myriad walls of the spheres. From this, it is really not clear just what is being measured within the few millimeters penetrated by microwave wavelengths.

Because of the complications of the air-sea interactions, the flux that is radiated from the quiet sea seems to be reported varying between the seawater temperature and the prevailing air temperature.

If microwave wavelengths cannot suitably penetrate a medium, such as seawater, then how can its intrinsic properties be measured? These are the questions, these are the conditions, these are the imponderables that affect confidence in the flux measurements from the quiet sea.

EXHIBITS 1, 2, AND 3 - THE QUIET SEAS

Exhibits 1, 2, and 3 are the measured flux responses for three quiet seas: Sargasso Sea (Orbit 801), Equator (Orbit 1492), and Indian Ocean (Orbit 1492). Each Exhibit summarizes the responses for the five frequencies and for the vertical and horizontal polarizations at each frequency--across 1 swath [see Note (5)].

The plots shown in the Exhibits are self-explanatory when combined with the foregoing discussion material and with the benefit of the clarifications given in the footnotes.

For each of the three quiet seas there is a

... local map showing the detailed geographical position of the microwave flux image (a rectangle) that the plotted swath was taken from. The swath is identified by a dashed line.

... visible and/or infrared image (DMSP or NOAA) that shows the prevailing cloud conditions during the time of the satellite overflight. Typically, the cloud images are taken within a few hours of the time of the overflight. On each of the cloud images is superposed a seamark in the form of an ellipse O--in most cases--or as a series of concentric circles in others that identify the exact position of the center of the plotted swath (the dashed line).

... computation of the expected value for the thermodynamic background temperature, T_B as referenced to the phase center (see Note [6] of the imaging antenna).

As has been previously stated, the plots in the Exhibits show only the primitive responses of the receivers.

The information that is displayed in the plots is:

... the change in the magnitude of the digital counts as they are affected by relative gain at each frequency.

... the magnitude and the pattern of the polarization rotation that is caused by rotation of the collector with respect to the feed.

... the difference between the horizontal and the vertical polarizations--point by point.

... the total range of the plotted points for both the vertical and the horizontal polarizations.

... the mean value for the horizontal and vertical plots. Mean values are separately shown near the right margins.

... the correlation coefficient, R. It expresses the fraction of the changes in the horizontal channel that are explained by the changes in the vertical channel.

... the gain scale factor which is given for the purpose of converting small differences in the digital counts into equivalent thermodynamic temperature units. The converted units should be regarded as approximations. Only small differences in digital count units should be used for the conversions.

... the incidence angle. A constant which is equal to 48.77 degrees.

Investigators are also burdened with the interpretation of the quiet sea plots--especially as they may be locally affected by surface roughness and/or attenuating media in the atmosphere.

It is of critical importance to understand that the plots of the quiet seas are pristine in character--that is, the output responses of the receivers have not been modified or processed in any way. Conceptually, the plotted data appear as they emerge from the receiver detectors--and have only been transformed into digital quantities.

Further, the data are taken and plotted across the extent of 1 swath, a distance of 603 km, as projected on the surface of the Earth. The elapsed time for a swath is two seconds. There are 47 discrete pointing positions across the interval of a swath. The spacing between the pointing positions is variable because the scanning waveform is a sinusoid.

Exhibit 4 describes the microwave responses for a cloudy, windy sea--near Graham and Vancouver Islands on the west coast of Canada. The geographical area is shown in Figure E4-1.

The plotted swath is shown as a dashed line within the rectangular section. The eastern end of the swath is only 120 kilometers from the southern tip of Graham Island.

Two NOAA Data Buoys are shown within the rectangle. Meteorological and Oceanographic Station PAPA is shown at 50 North Latitude/145 West Longitude. NOAA 101--The Oceanographer, a ship, is located at Station PAPA.

The weather conditions are expressed for the area by the visible and infrared photographs. See Figures E4-2 and E4-3. A circle is superposed on the photographs and it appears in the upper left-hand quadrants. An ellipse marks the center of the plotted swath. The eastern portion of the swath extends into the heavy stratus cloudform that is shown along the coast near Graham Island. The western portion of the swath extends into a relatively clear area of the Pacific.

The NOAA Data Buoys and Station PAPA provided the wind-speed conditions at the sea surface for the time of the overflight. The mean wind speed is given in the legend on the plots. The character of the wind is described in Table E4-1.

The reflected sun angle (RSA) is only 6.1 degrees from the axis of the downwelling path. Because of the roughness of the sea, the solar flux is sufficiently scattered as it arrives at the collecting aperture that it does not appear in any of the plots.

On the 37-GHz plots, the digital counts for the horizontal and vertical channels increase together and nearly merge near the pointing-axis position of -20 degrees. This phenomenon is coincident with the occurrence of the dense cloud pattern seen in the visible and infrared photographs. On the western portion of the swath, the horizontal and vertical channel responses generously separate.

The 6-GHz plots are unaffected by the stratus clouds. Also, they are unaffected by the close proximity to land: this is because of the low antenna gain. The inward cusping of the horizontal and vertical plots are manifestations of the effects of the rotation of the collecting aperture with respect to the feed.

At 10 GHz, there are only slight increases in the amplitude of the plots as affected by the dense cloud pattern.

The plotted data for the five frequencies and with two polarizations are in the same format as for the quiet seas.

ENDNOTES

[1] The microwave imager on the Nimbus-7 spacecraft produces a symmetrical scan pattern that is centered on the ground track of the spacecraft. The axis-of-maximum-gain is directed forward of the spacecraft and it maintains a constant angle of coincidence of 50.3 degrees.

The microwave imager on the SEASAT spacecraft has the zero-angle scan position offset from the ground track of the spacecraft by about 22 degrees. This offset is required to bring about better coincidence of the observed Earth areas among sensors on the spacecraft. Also the axis-of-maximum-gain is directed in the rear direction of the spacecraft at a constant angle of incidence of 48.8 degrees.

[2] The axis-of-maximum-gain, or the on-axis-gain as it is sometimes called, is defined as the central axis of the major lobe of the directional diagram for the antenna. It is also regarded as the pointing axis for the collecting aperture.

Microwave power is transferred and collected by the relative gain properties of the collecting aperture. For this reason, gain is a quantity of critical importance in this monograph.

The expression for gain is given by

$$G_o = (4\pi A_c \eta)/\lambda^2, \text{ a dimensionless quantity}$$

where:

A_c = the area of the collecting aperture, m^2

η = solid-angle, main-beam efficiency

λ = operating wavelength, m.

[3] The correlation coefficient, R, expresses the fraction of the variations in the digital counts for the horizontal channel that are explained by the variations in the digital counts for the vertical channel.

The critical absolute value for the correlation coefficient is 0.28--which is based on 47 degrees of freedom with 90% confidence intervals [3]. The proper statistical interpretation for the critical absolute value conveys the expectation that there is a 90% probability that a correlation coefficient as high as 0.28 will not occur by accident. It implies that there is a 10% chance of being wrong.

[4] A detailed discussion of the factors that cause clutter as it is evidenced in orbiting microwave receivers is given in [2].

[5] The scanning mechanism on the spaceborne receiver produces a sector scan (Figure 2) with a sinusoidal waveform.

There are two independent 37-GHz receivers that are connected to the vertical and horizontal ports of the multifrequency feed assembly. Because of this electrical arrangement the 37-GHz channels remain coincident and independent at all times.

At all the other frequencies, there is only one receiver. An RF switch in the front end of each receiver alternately connects the input terminals of the receiver to the horizontal and vertical ports of the multifrequency feed on alternate swaths of the sinusoidal scan--that is, the horizontal and vertical polarizations occur on alternate swaths of the continuous sinusoidal scan.

The software for the quiet sea observations includes an interpolation subroutine that brings all of the vertical and horizontal channels, at each frequency, into coincidence with the vertical 37-GHz channel. For this reason, the vertical 37-GHz channel is adopted as a preference when critical comparisons are being made.

[6] The antenna configuration is described as an articulating collector with a fixed multifrequency feed assembly--an offset prime-focus antenna. Within the body of the feed structure is a finite, mathematically defined point where all of the flux that is collected by the articulating aperture is focused. In the argot of antenna design, it is called the phase center of the antenna. The phase center is common to all frequencies and polarizations.

REFERENCES

[1] J. M. Stacey, Microwave Blackbodies for Spaceborne Receivers, JPL Publication 85-10, March 1, 1985.

[2] J. M. Stacey, Power Transfer from Natural Emitters to Collecting Apertures at Microwave Wavelengths, JPL Publication 84-48, December 1, 1984.

[3] E. L. Crow, F. A. Davis, M. A. Maxfield, Statistics Manual, Page 241, Dover Publications, N. Y., 1960.

EXHIBIT 1

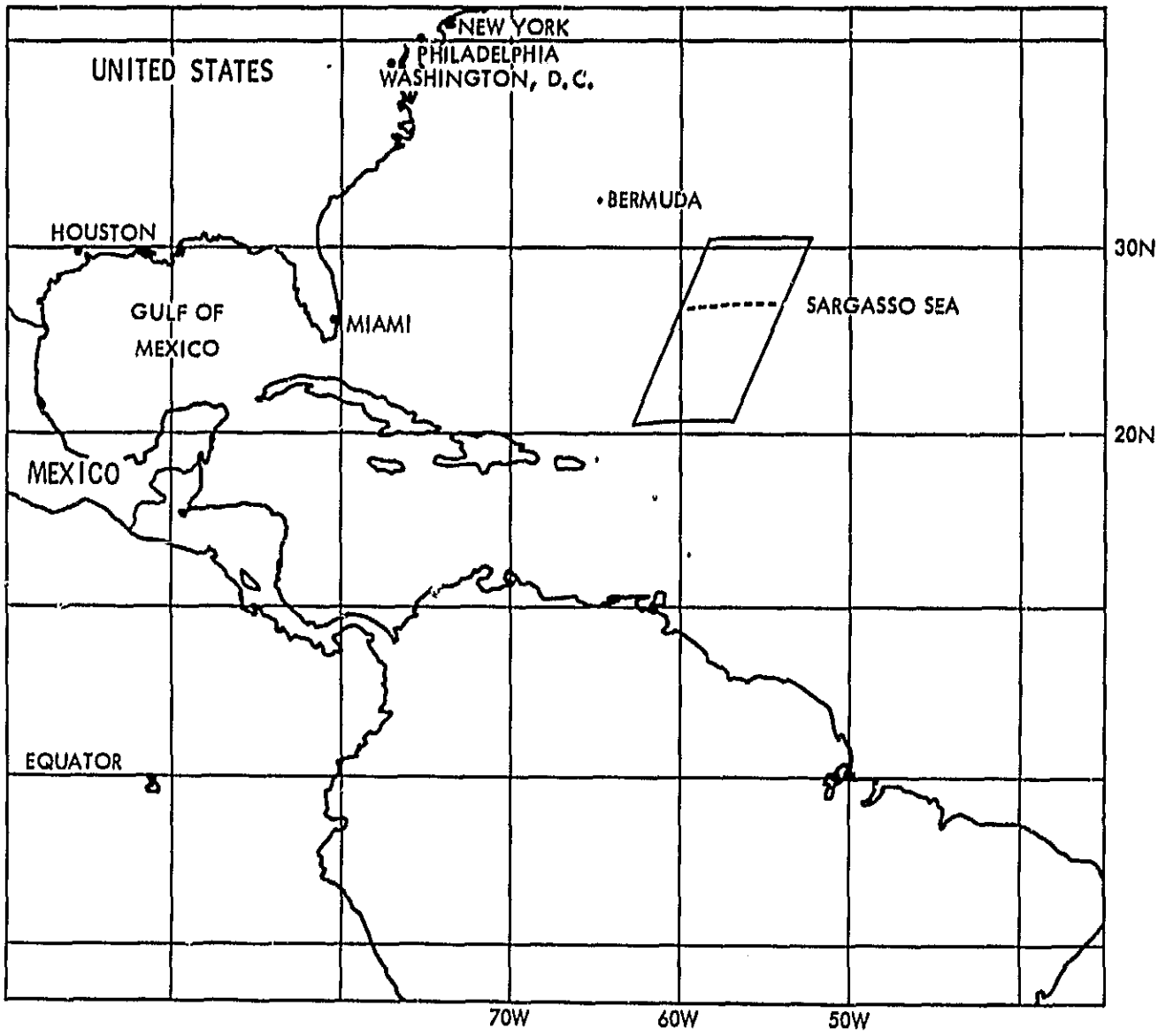

Figure E1-1. The Sargasso Sea - A Quiet Sea

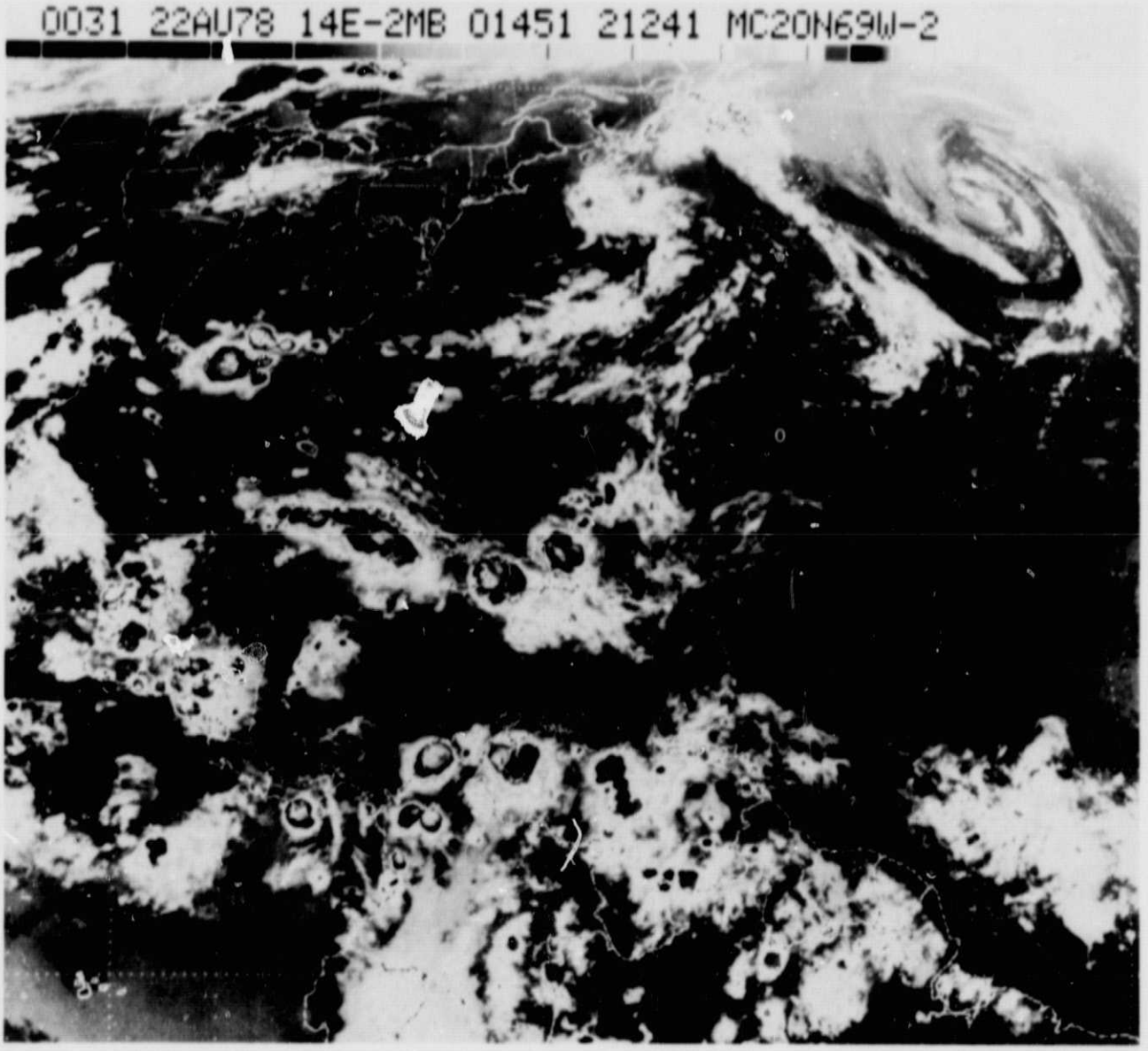

Figure E1-2. An Infrared Image of the Cloud Cover Over the Sargasso Sea. (The small white ellipse, slightly to the right of center, is the center position (scan angle = 0 degrees) for the measured swath shown by the dashed line in Figure E1-1.)

$$T_B = \underbrace{\frac{T_{COSMIC}}{L_{ad}\,L_{surf}\,L_{au}}}_{[\text{COSMIC}]} + \underbrace{\frac{T_{ad}\,(L_{ad}-1)}{L_{ad}\,L_{surf}\,L_{au}}}_{[\text{DOWNWELLING}]} + \underbrace{\frac{T_{surf}\,(L_{surf}-1)}{L_{surf}\,L_{au}}}_{[\text{SURFACE}]} + \underbrace{\frac{T_{au}\,(L_{au}-1)}{L_{au}}}_{[\text{UPWELLING}]}\ , \text{ KELVINS}$$

$$= \frac{2.7}{(1.08)(1.54)(1.08)} + \frac{280\,(1.08-1)}{(1.08)(1.54)(1.08)} + \frac{290\,(1.54-1)}{(1.54)(1.08)} + \frac{280\,(1.08-1)}{(1.08)}\ , \text{ KELVINS}$$

$$= (1.5) + (12.47) + (94.16) + (20.74)\ , \text{ KELVINS}$$

$$= 128.87 \text{ KELVINS}$$

ASSUMPTIONS FOR CLEAR WEATHER AT MID - LATITUDE:

$T_{COSMIC} = 2.7$ K

$L_{ad} = L_{au} = 0.35$ dB (1.08)

$\epsilon = 0.35$ (ARBITRARY POLARIZATION)

$L_{surf} = \frac{1}{1-\epsilon} = 1.54$ (INCLUDES ESTIMATE FOR LOSSES IN THE SKIN DEPTH FOR LIQUID SEAWATER, FOAM, BUBBLES, MARINE LIFE, OIL FILMS, SEAWEED, CHEMICAL POLLUTANTS, ETC.)

$T_{ad} = T_{au} = 280$ K

$T_{surf} = 290$ K

Figure E1-3. The Thermodynamic Temperature Structure of the Background Temperature T as Referenced to the Phase-Center of the Antenna. A Clear Weather Model for Mid-Latitudes at 8-mm Wavelength.

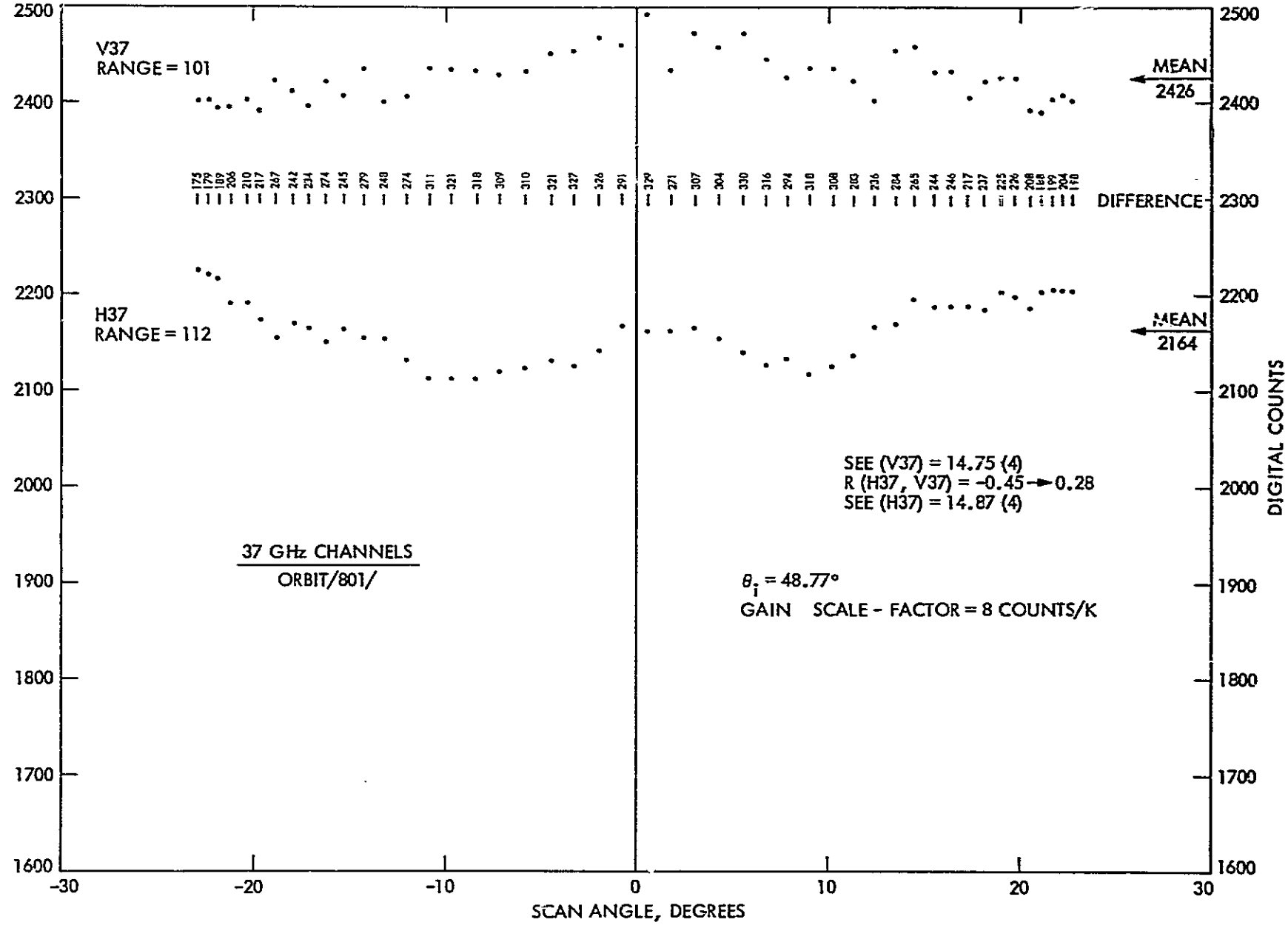

Figure E1-4. Sargasso Sea Channels at 37 GHz

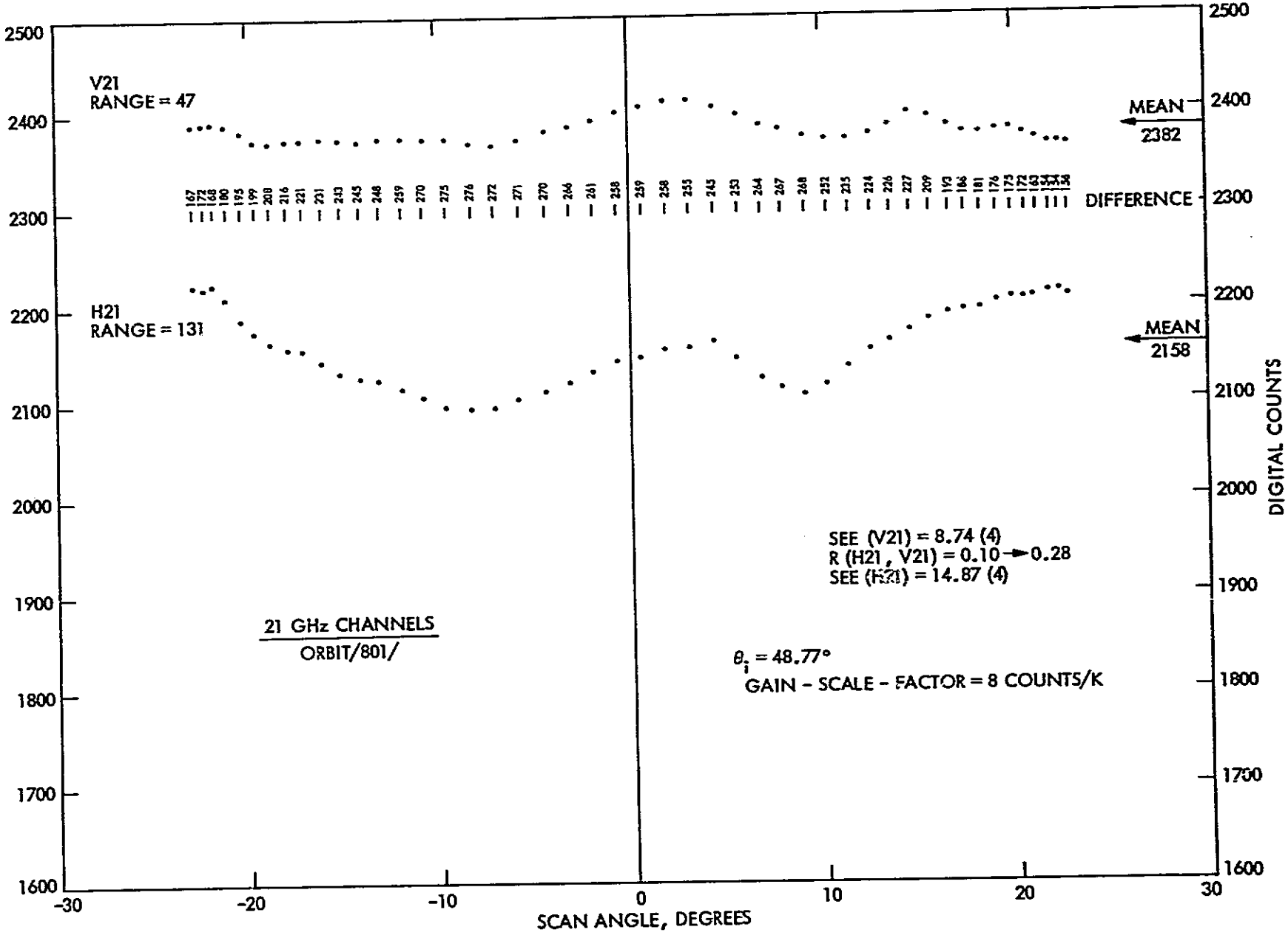

Figure E1-5. Sargasso Sea Channels at 21 GHz

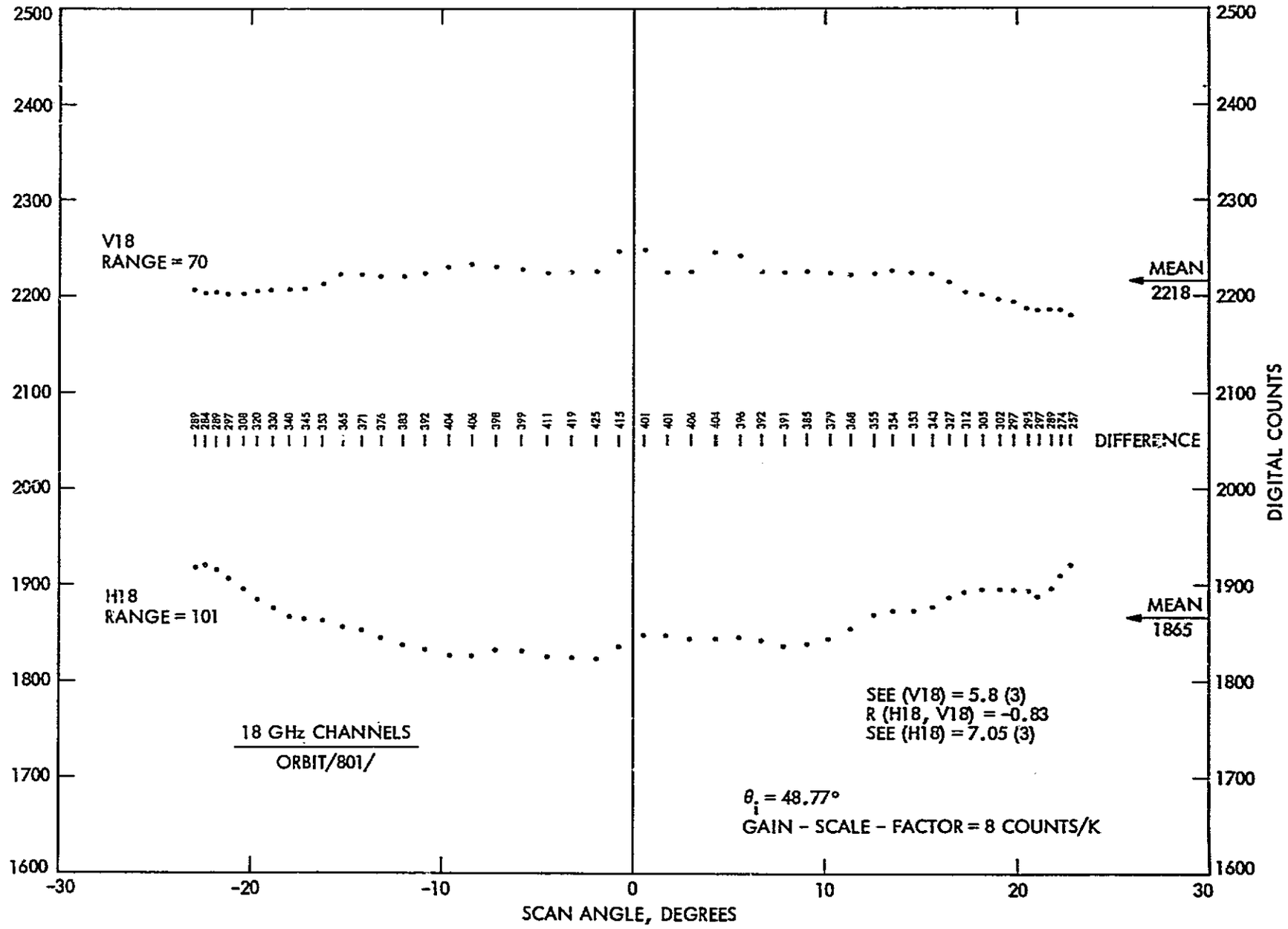

Figure E1-6. Sargasso Sea Channels at 18 GHz

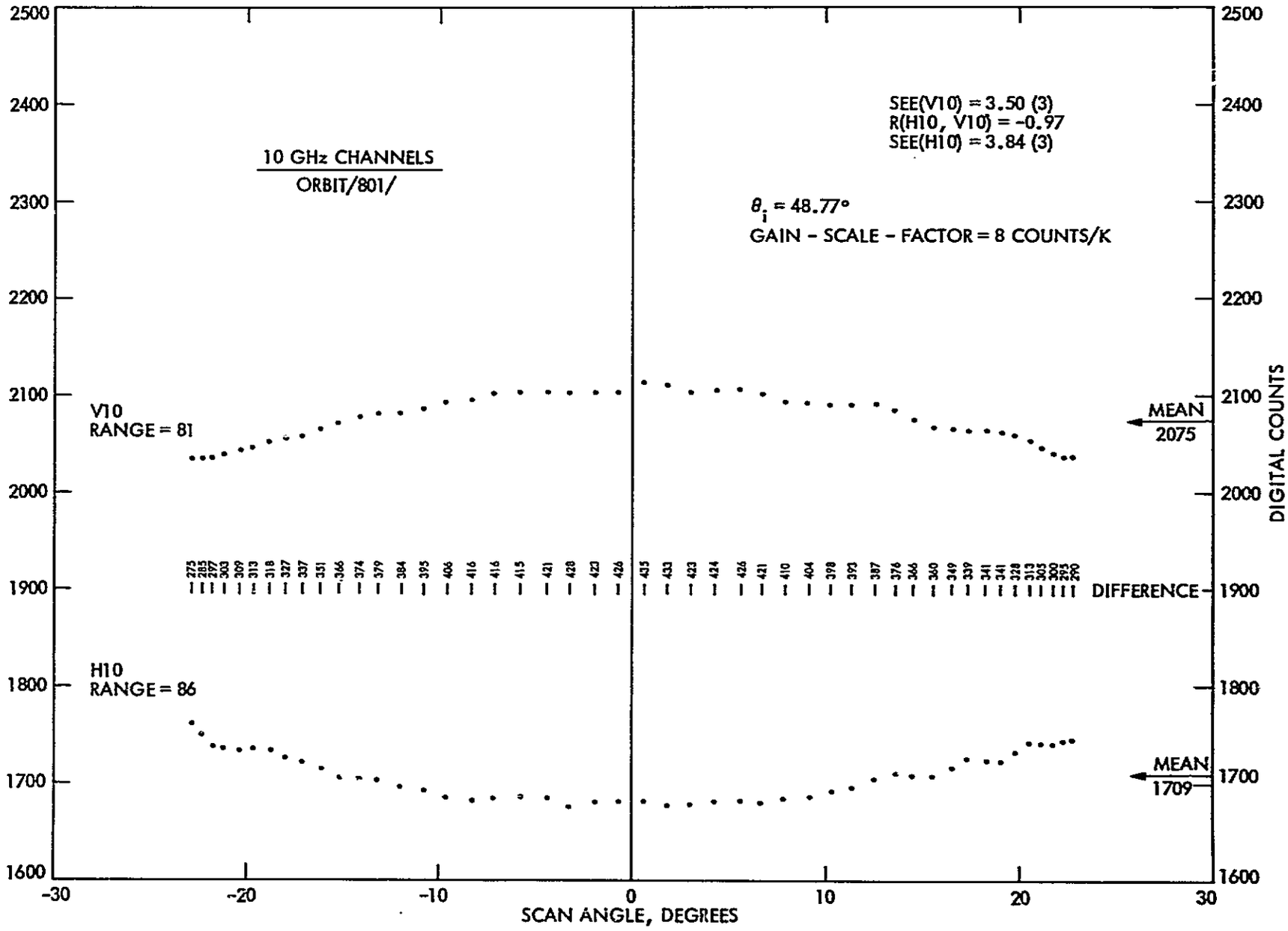

Figure E1-7. Sargasso Sea Channels at 10 GHz

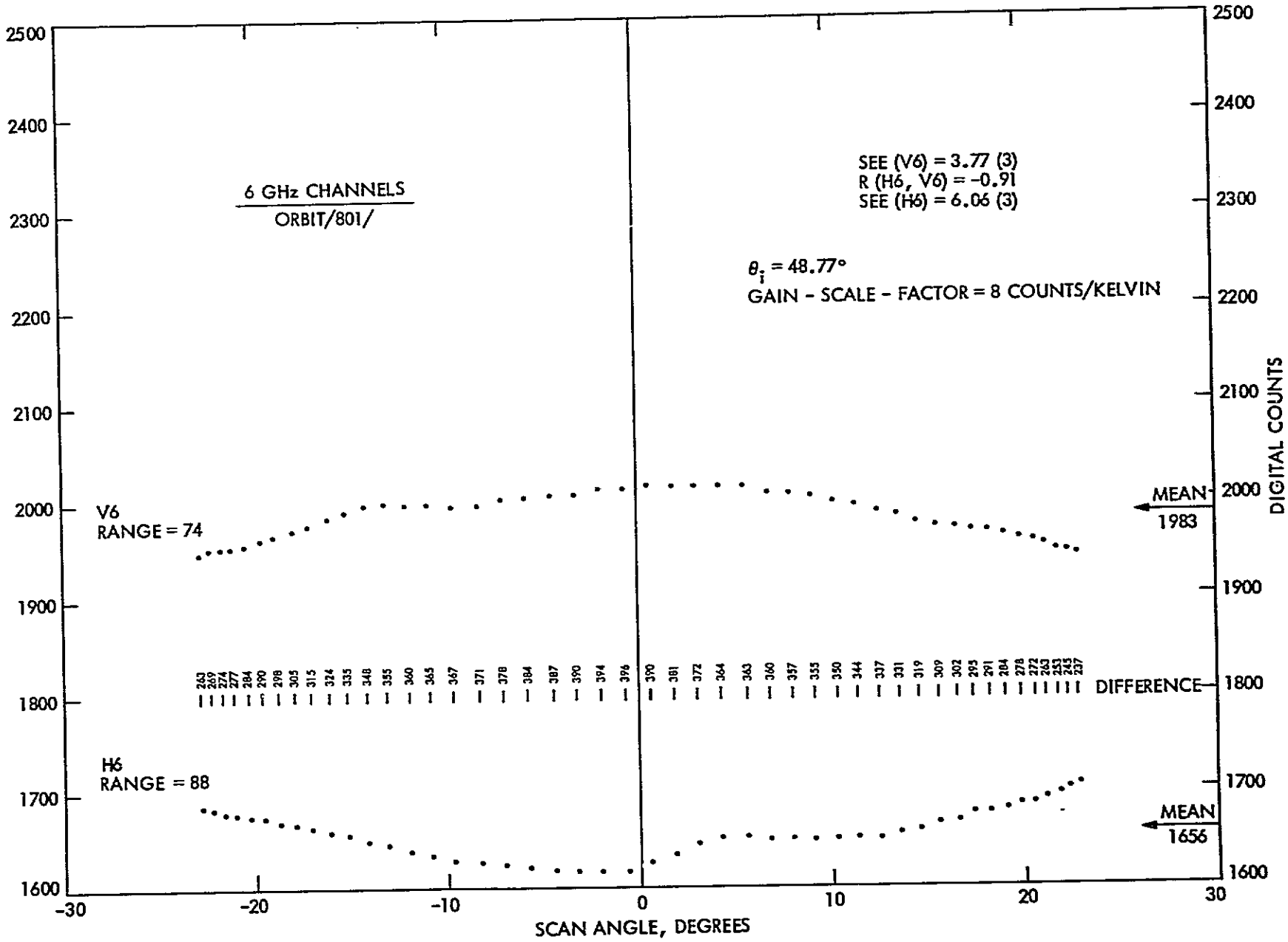

Figure E1-8. Sargasso Sea Channels at 6 GHz

EXHIBIT 2

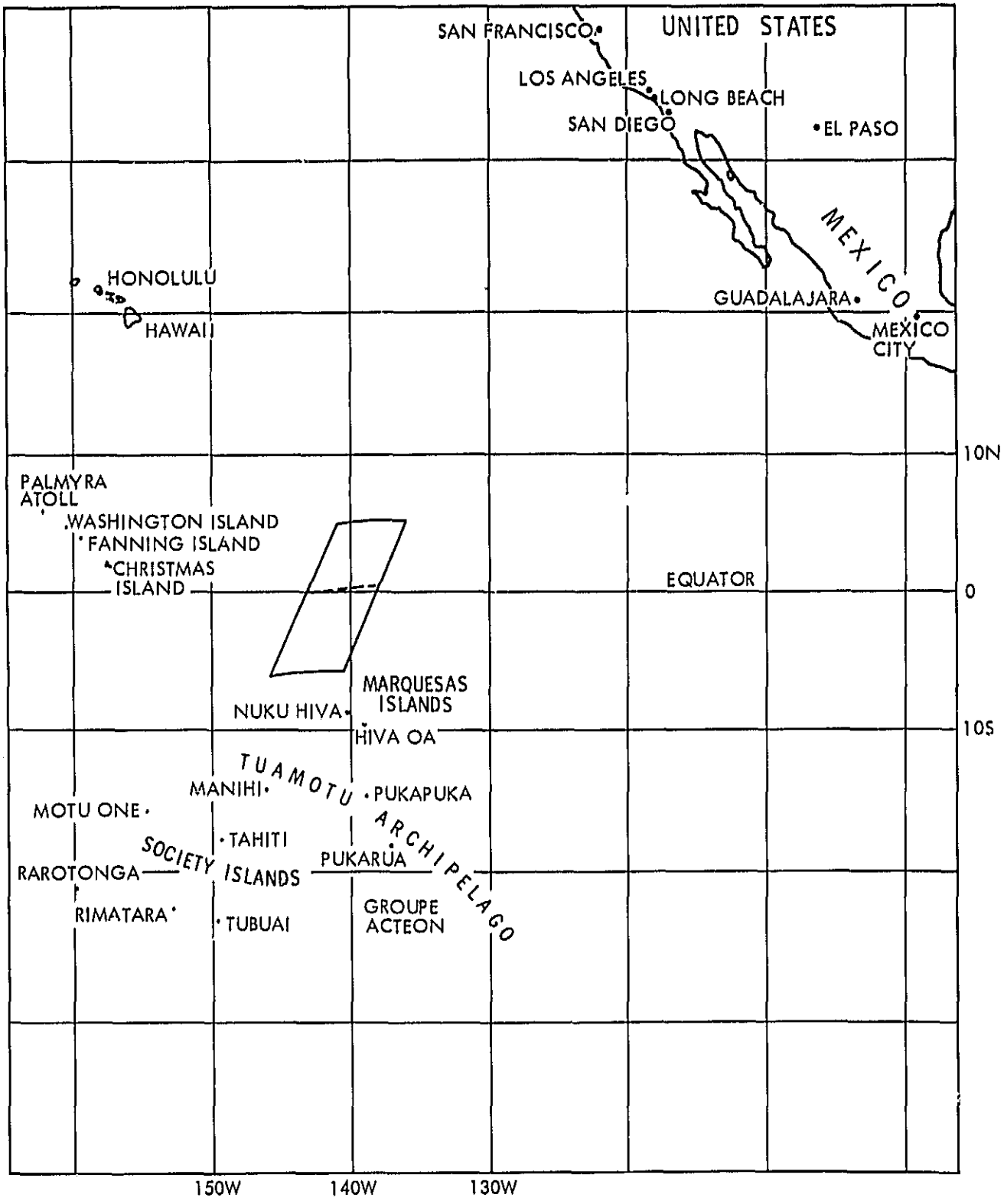

Figure E2-1. The Equator Area - A Quiet Sea

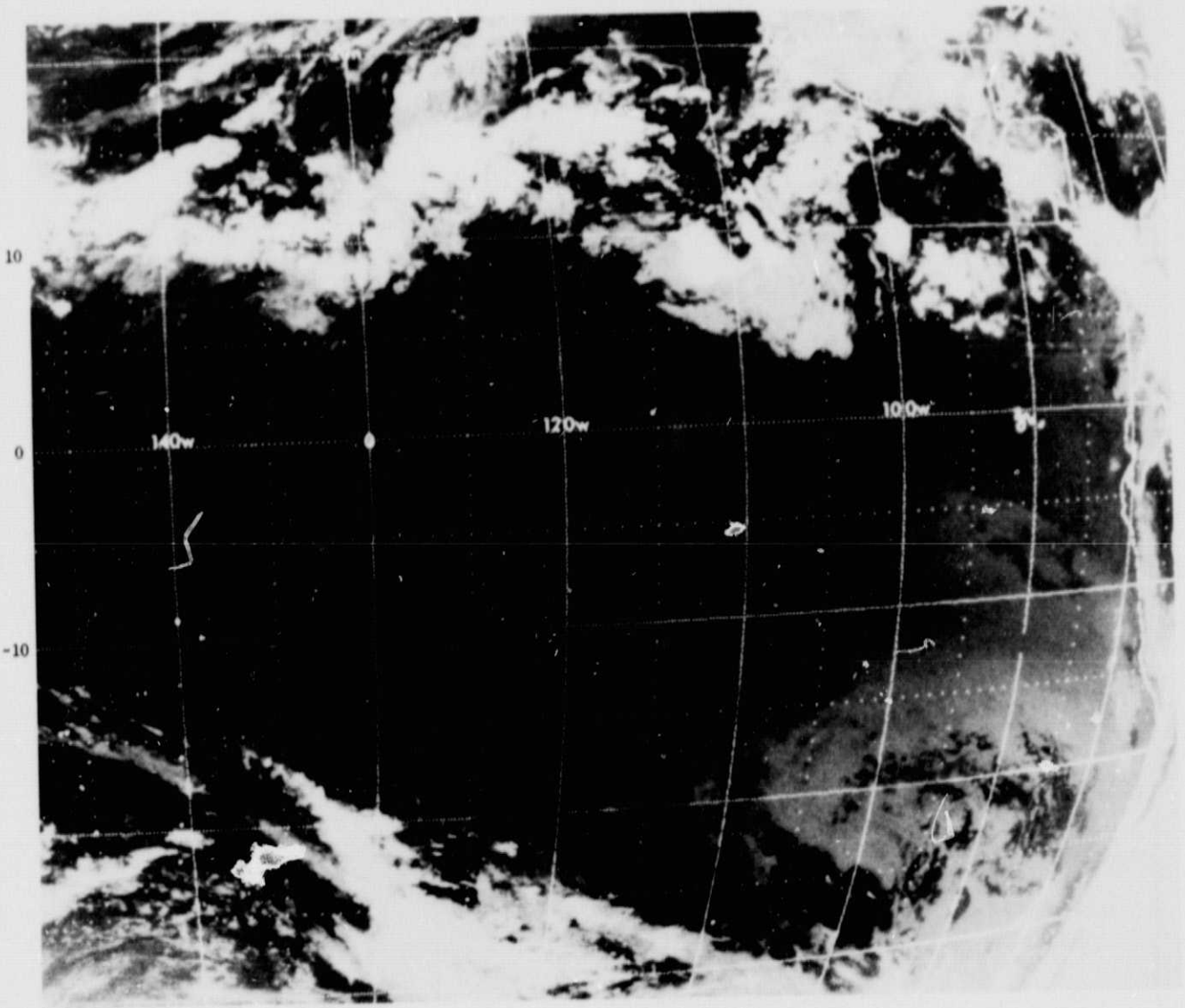

Figure E2-2. An Infrared Image of the Equator Area. (The center of the measured swath (scan angle = 0 degrees), as shown by the dashed line in Figure E2-1, is coincident with 0 N Latitude/ 140 W Longitude.)

$$T_B = \underbrace{\frac{T_{COSMIC}}{L_{ad}\,L_{surf}\,L_{au}}}_{[\text{COSMIC}]} + \underbrace{\frac{T_{ad}\,(L_{ad}-1)}{L_{ad}\,L_{surf}\,L_{au}}}_{[\text{DOWNWELLING}]} + \underbrace{\frac{T_{surf}\,(L_{surf}-1)}{L_{surf}\,L_{au}}}_{[\text{SURFACE}]} + \underbrace{\frac{T_{au}\,(L_{au}-1)}{L_{au}}}_{[\text{UPWELLING}]}\text{, KELVINS}$$

$$= \frac{2.7}{(1.08)(1.54)(1.08)} + \frac{280\,(1.08-1)}{(1.08)(1.54)(1.08)} + \frac{290\,(1.54-1)}{(1.54)(1.08)} + \frac{280\,(1.08-1)}{(1.08)}\text{, KELVINS}$$

$$= (1.5) + (12.47) + (94.16) + (20.74)\text{, KELVINS}$$

$$= 128.87 \text{ KELVINS}$$

ASSUMPTIONS FOR CLEAR WEATHER AT MID - LATITUDE:

$T_{COSMIC} = 2.7$ K

$L_{ad} = L_{au} = 0.35$ dB (1.08)

$\epsilon = 0.35$ (ARBITRARY POLARIZATION)

$L_{surf} = \frac{1}{1-\epsilon} = 1.54$ (INCLUDES ESTIMATE FOR LOSSES IN THE SKIN DEPTH FOR LIQUID SEAWATER, FOAM, BUBBLES, MARINE LIFE, OIL FILMS, SEAWEED, CHEMICAL POLLUTANTS, ETC.)

$T_{ad} = T_{au} = 280$ K

$T_{surf} = 290$ K

Figure E2-3. The Thermodynamic Temperature Structure of the Background Temperature T as Referenced to the Phase-Center of the Antenna. A Clear Weather Model for the Equator at 8-mm Wavelength. (This is the same model as given for a a mid-latitude in Figure E1-3.)

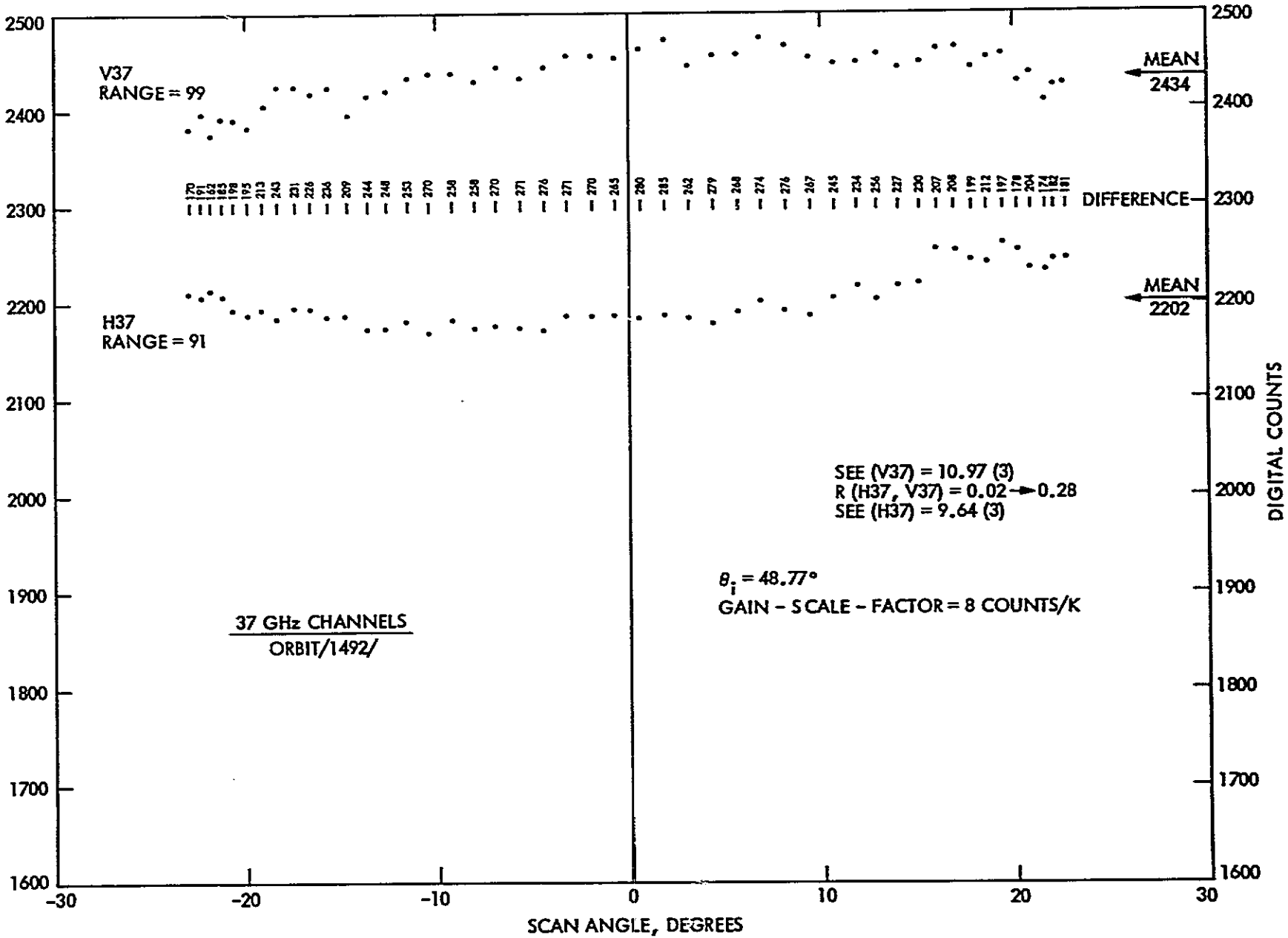

Figure E2-4. Equatorial Channels at 37 GHz

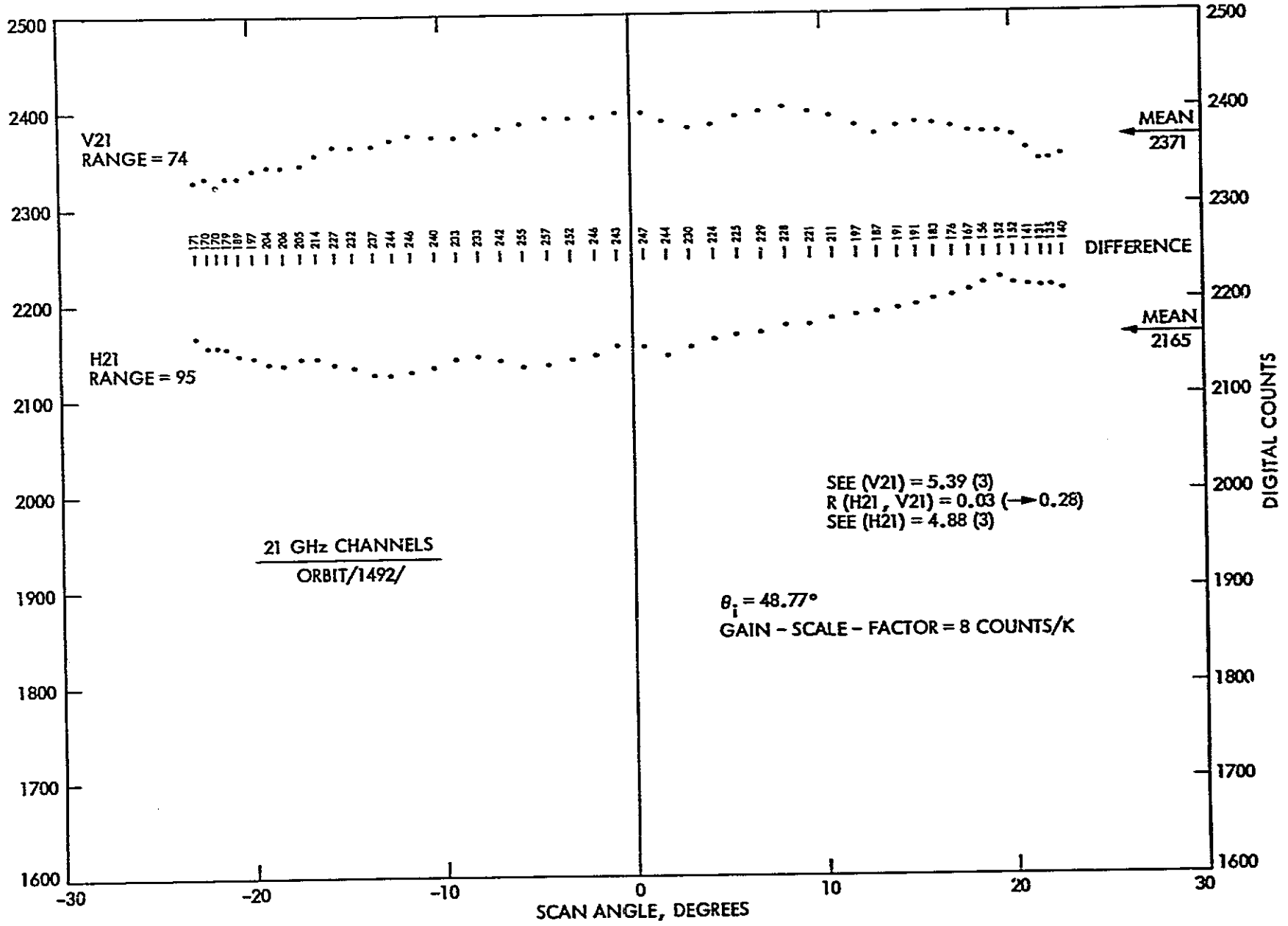

Figure E2–5. Equatorial Channels at 21 GHz

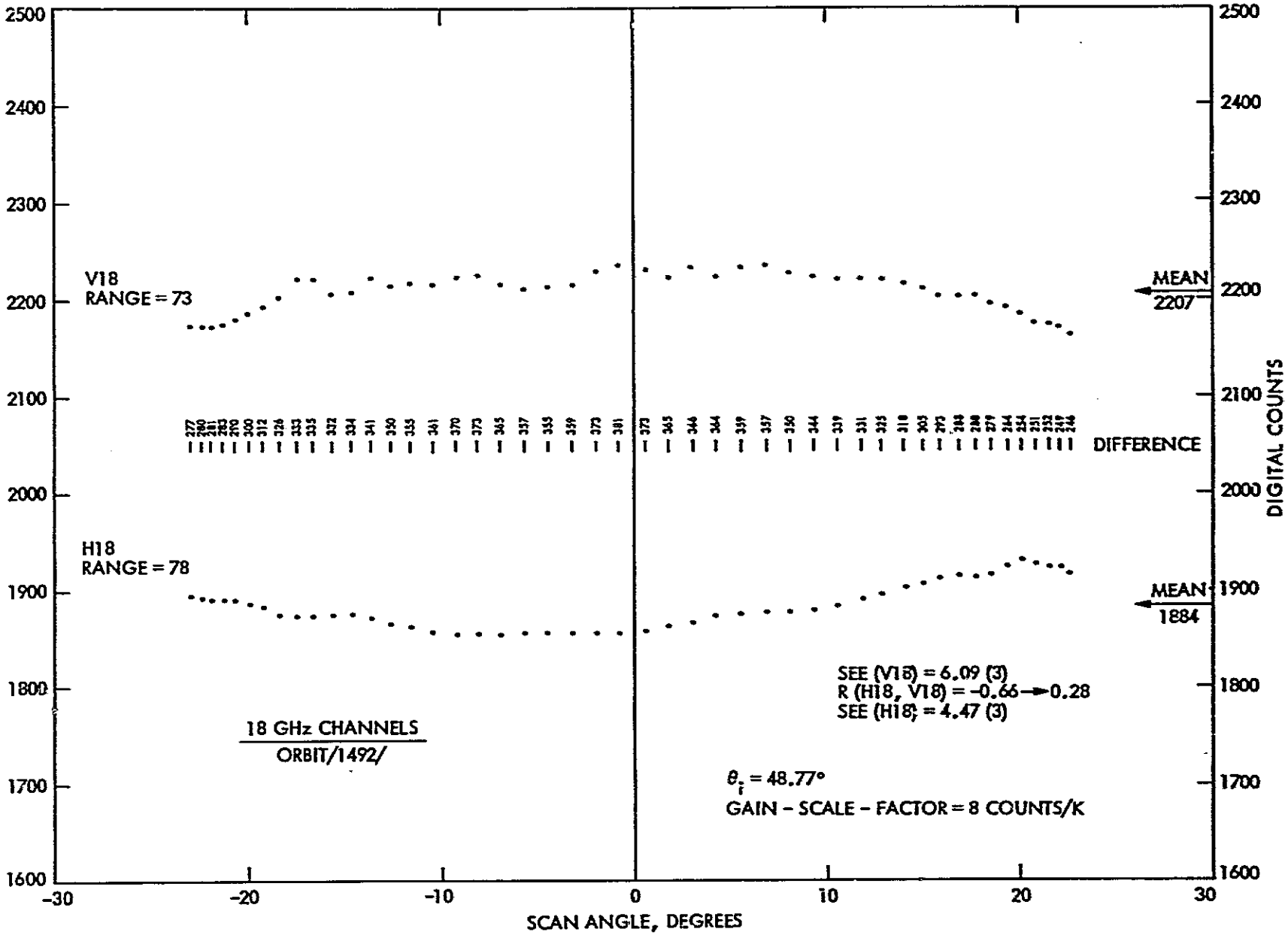

Figure E2-6. Equatorial Channels at 18 GHz

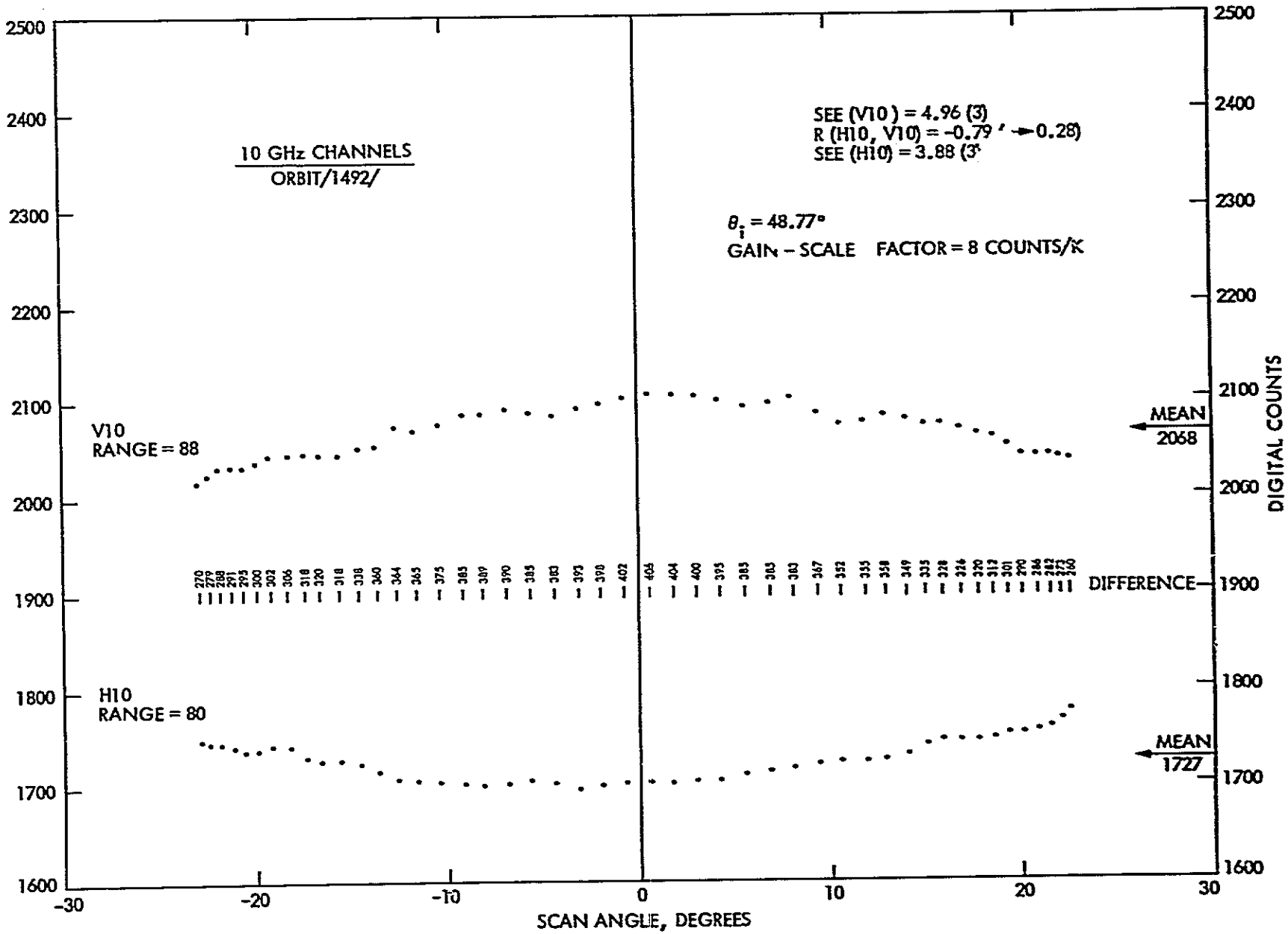

Figure E2–7. Equatorial Channels at 10 GHz

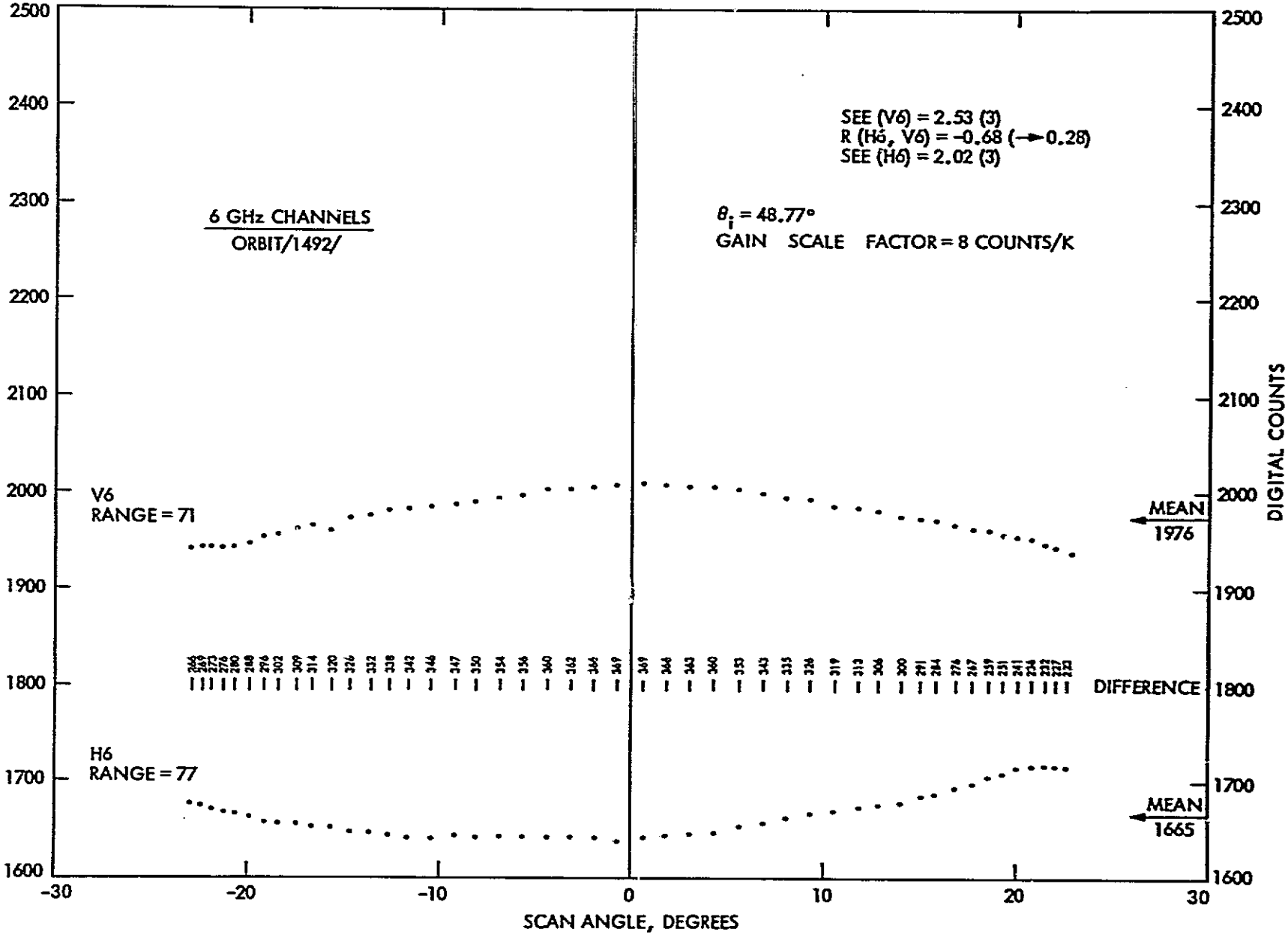

Figure E2-8. Equatorial Channels at 6 GHz

EXHIBIT 3

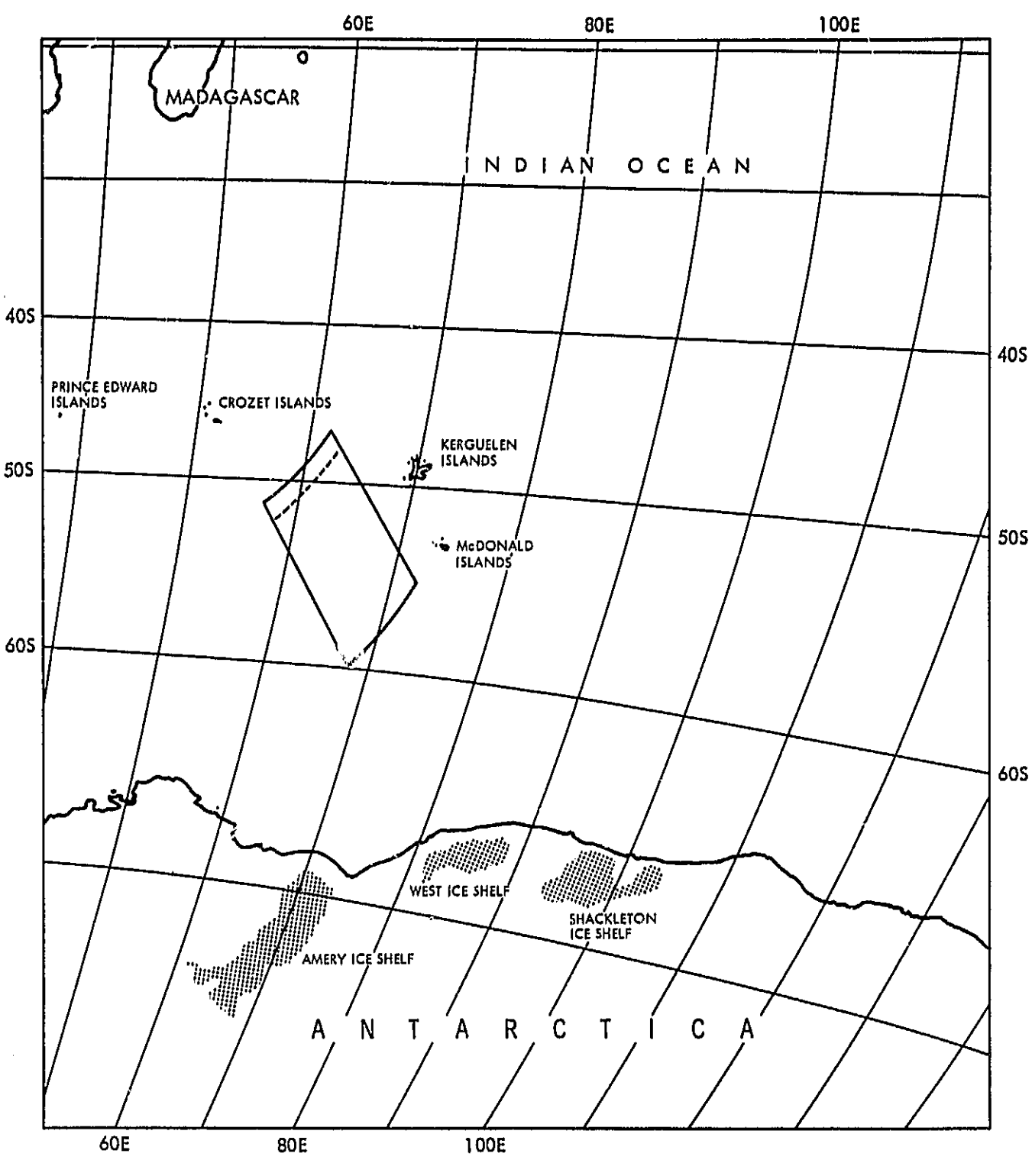

Figure E3-1. The Indian Ocean - Near Antarctica and Madagascar - A Quiet Sea

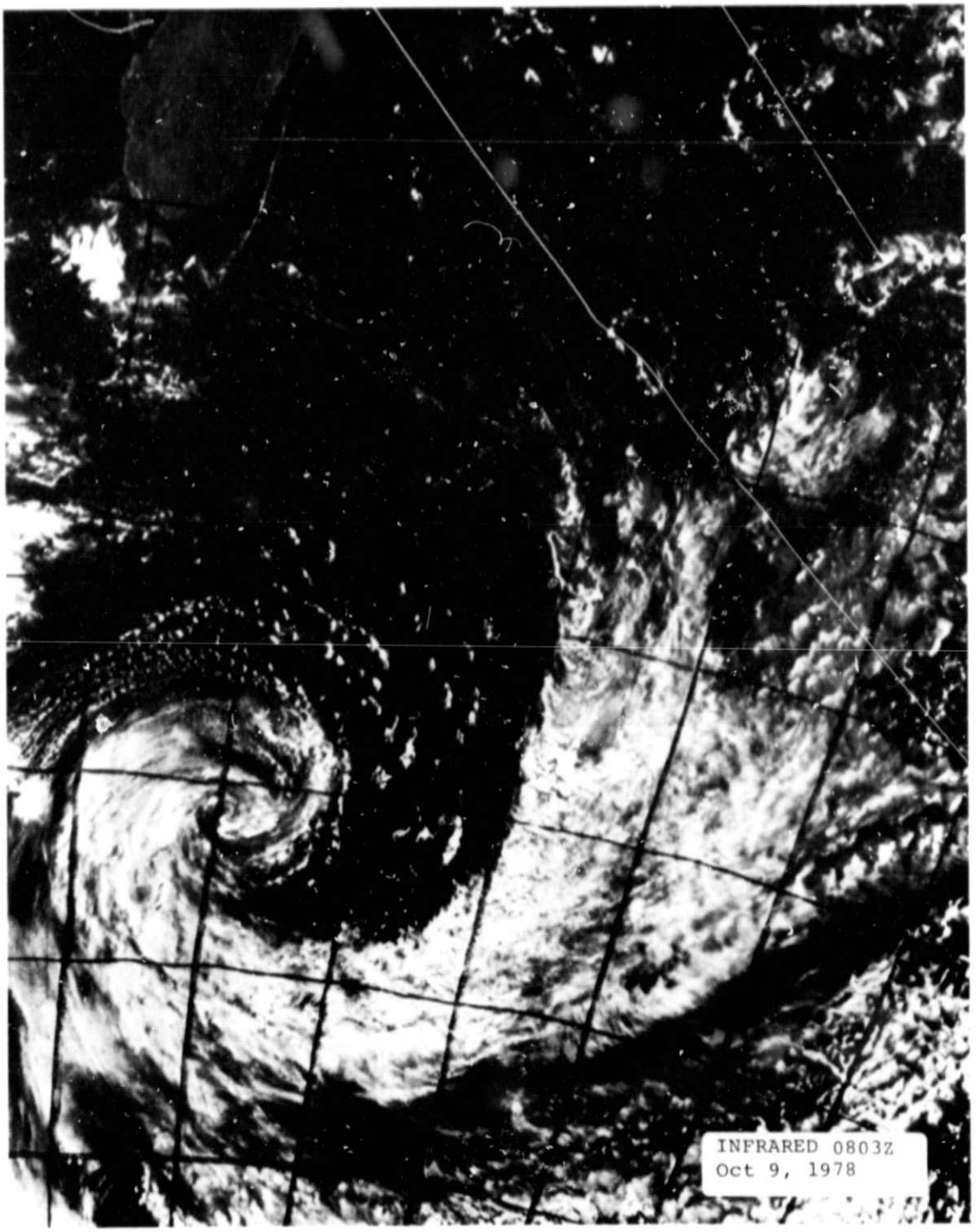

Figure E3-2. An Infrared Image of the Quiet Sea in the Indian Ocean. (The concentric circles near the bottom center are coincident with the center of the swath (scan angle = 0^{o}) as shown by the dashed line in Figure E3-1. The southern end of Madagascar is shown in the upper left.)

$$T_B = \underbrace{\frac{T_{COSMIC}}{L_{ad}\,L_{surf}\,L_{au}}}_{[\text{COSMIC}]} + \underbrace{\frac{T_{ad}\,(L_{ad}-1)}{L_{ad}\,L_{surf}\,L_{au}}}_{[\text{DOWNWELLING}]} + \underbrace{\frac{T_{surf}\,(L_{surf}-1)}{L_{surf}\,L_{au}}}_{[\text{SURFACE}]} + \underbrace{\frac{T_{au}\,(L_{au}-1)}{L_{au}}}_{[\text{UPWELLING}]}\text{, KELVINS}$$

$$= \frac{2.7}{(1.13)(1.54)(1.13)} + \frac{273\,(1.13-1)}{(1.13)(1.54)(1.13)} + \frac{(285)(1.54-1)}{(1.54)(1.13)} + \frac{273\,(1.13-1)}{(1.13)}\text{, KELVINS}$$

$$= (1.37) + (18.05) + (88.44) + (31.41)\text{, KELVINS}$$

$$= 139.27 \text{ KELVINS}$$

ASSUMPTIONS FOR LOSSES IN DOWNWELLING AND UPWELLING PATH FOR OXYGEN, WATER VAPOR, AND A WATER CLOUD.

$T_{COSMIC} = 2.7$ K

CLOUD ATTENUATION = 0.163 dB (0.2 gm/m^3 DENSITY)

OXYGEN AND WATER VAPOR ATTENUATION 0.35 dB

$L_{ad} = L_{au} = 0.163 + 0.35 = 0.513$ dB (1.13)

$T_{ad} = T_{au} = 273$ K

$\epsilon = 0.35$ (ARBITRARY POLARIZATION)

$L_{surf} = \frac{1}{1-\epsilon} = 1.54$ (INCLUDES ESTIMATES FOR LOSSES IN THE SKIN DEPTH LIQUID SEAWATER, FOAM, BUBBLES, MARINE LIFE, OIL FILMS, SEAWEED, CHEMICAL POLLUTANTS, ETC.)

$T_{ad} = T_{au} = 273$ KELVINS

$T_{surf} = 285$ KELVINS

Figure E3-3. The Thermodynamic Temperature Structure of the Background Temperature T as Referenced to the Phase-Center of the Antenna. A Water-Cloud Model for a High Latitude, at 8-mm Wavelength.

Table E3-1. Cloud Emission Summary - Cumulus Water-Cloud Type - (0.2 gm/m^3)

FREQ (GHz)	λ (meters)	ATTEN. RATE K_c	CLOUD ALT. km	CLOUD THICKNESS km	CLOUD TEMP. K	ATTEN. dB	EMISSION TEMP. K
6.6	0.0452	0.0445	2	0.67	273	0.006	0.375
10.7	0.0281	0.1111	↓	↓	↓	0.015	0.935
18.0	0.0167	0.3024	↓	↓	↓	0.041	2.537
21.0	0.0143	0.4076	↓	↓	↓	0.055	3.414
37.0	0.0081	1.2139	↓	↓	↓	0.163	10.042
88.0	0.0034	6.4264	↓	↓	↓	0.861	49.131

$$K_c = 0.001169\ F_{GHz}^{1.9235},\ dB/km/gm/m^3$$

→ FOR RAYLEIGH DROP SIZE AT 273 K

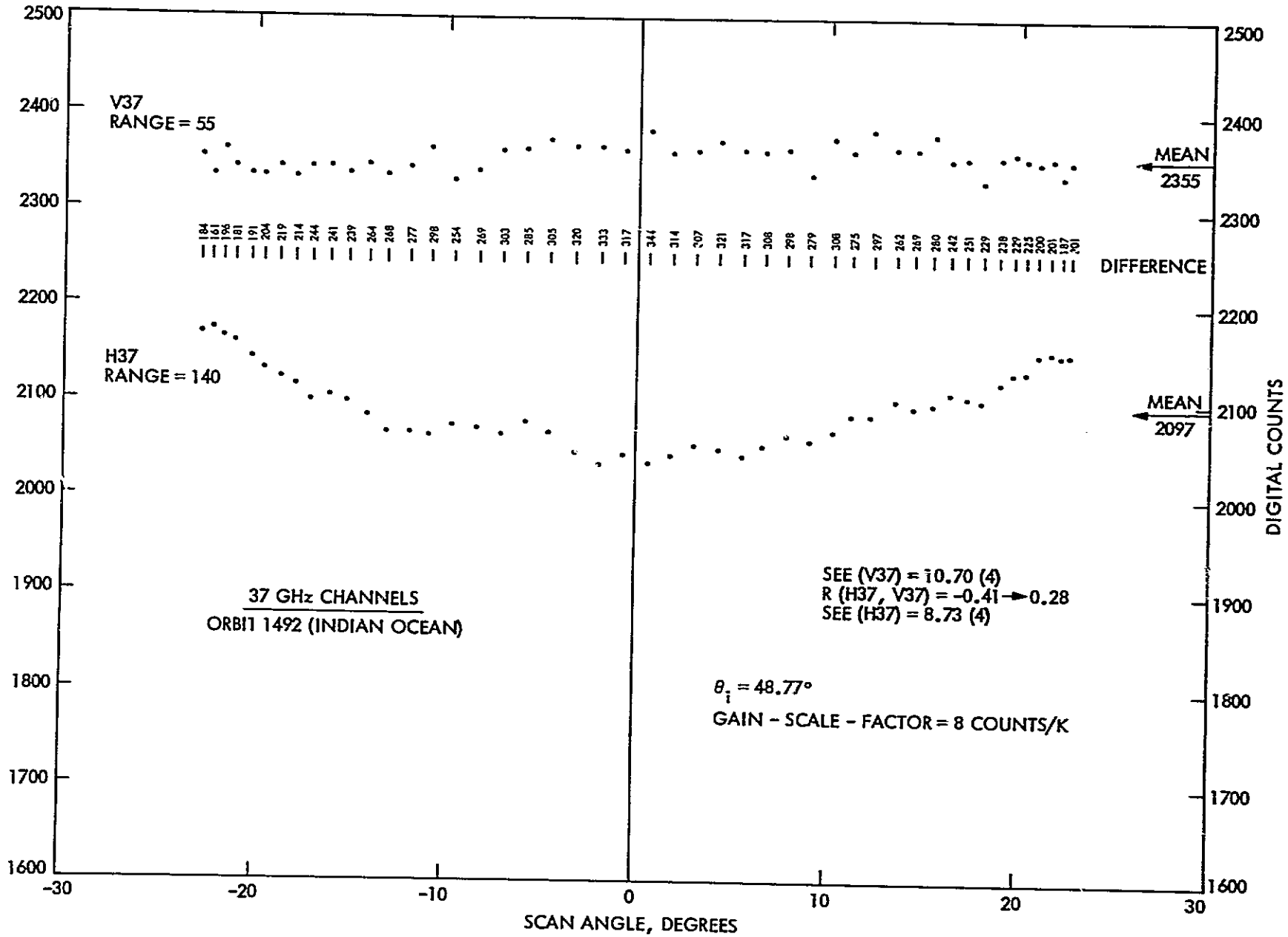

Figure E3-4. Indian Ocean 37-GHz Channels

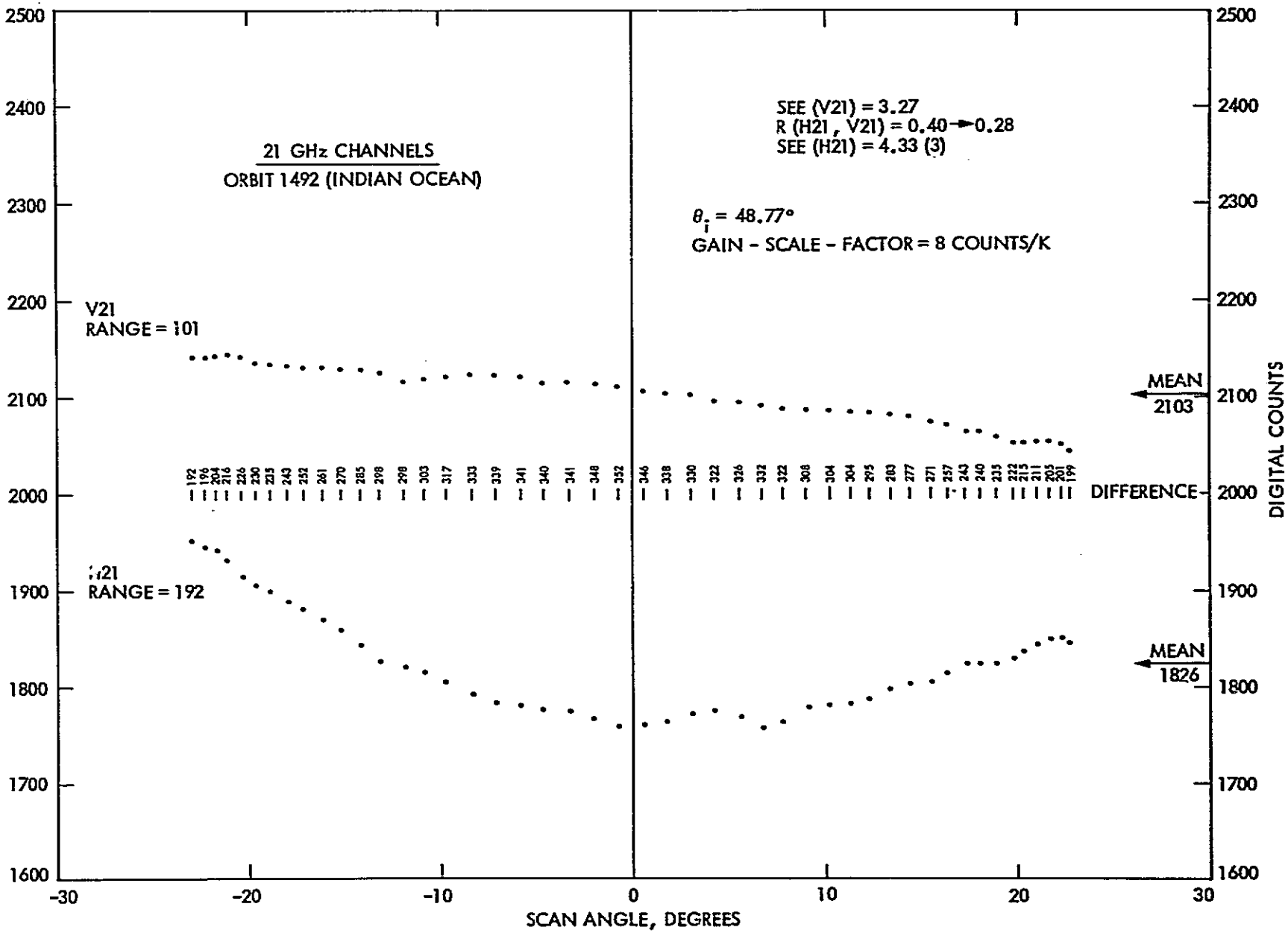

Figure E3-5. Indian Ocean 21-GHz Channels

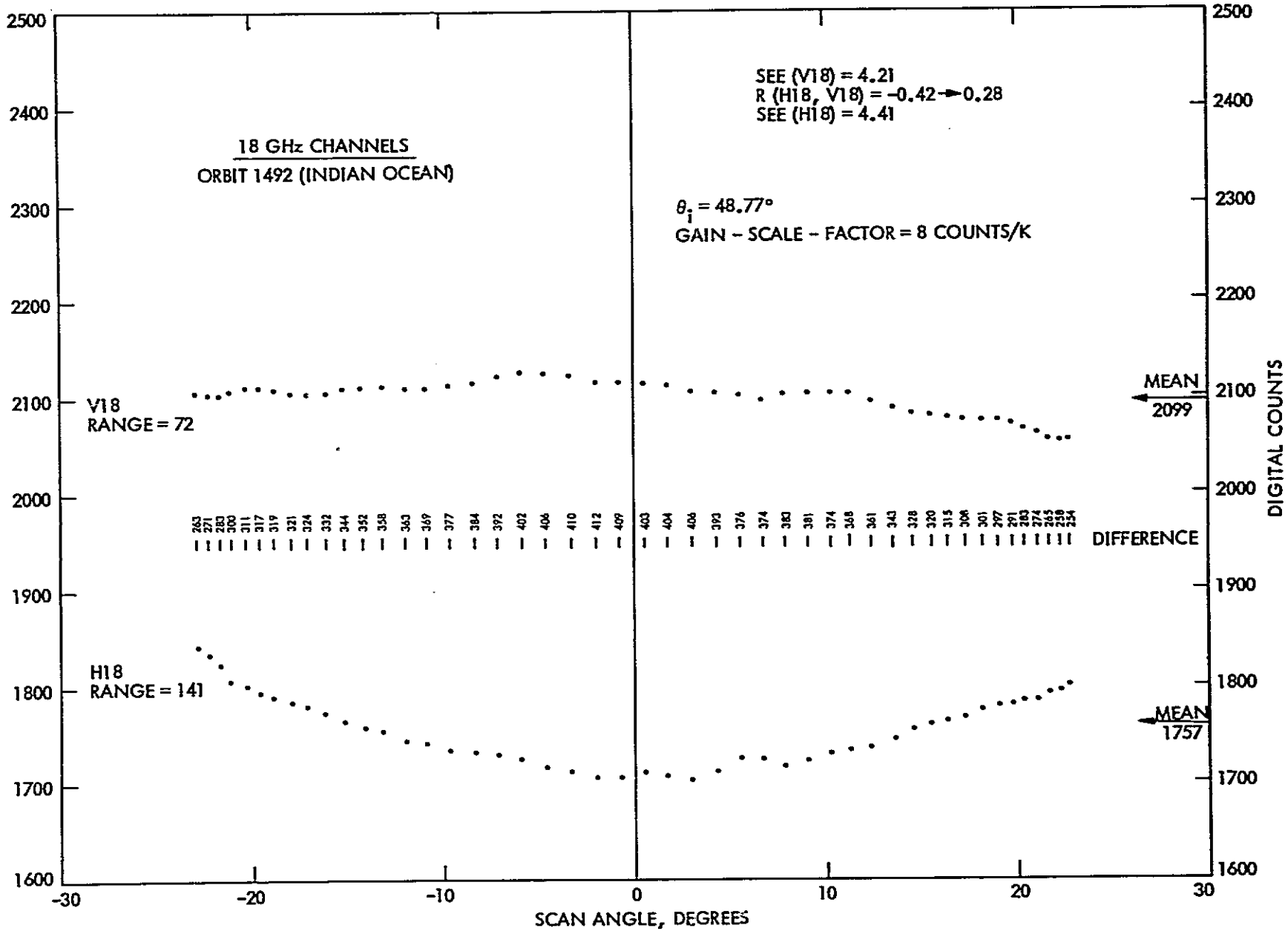

Figure E3-6. Indian Ocean 18-GHz Channels

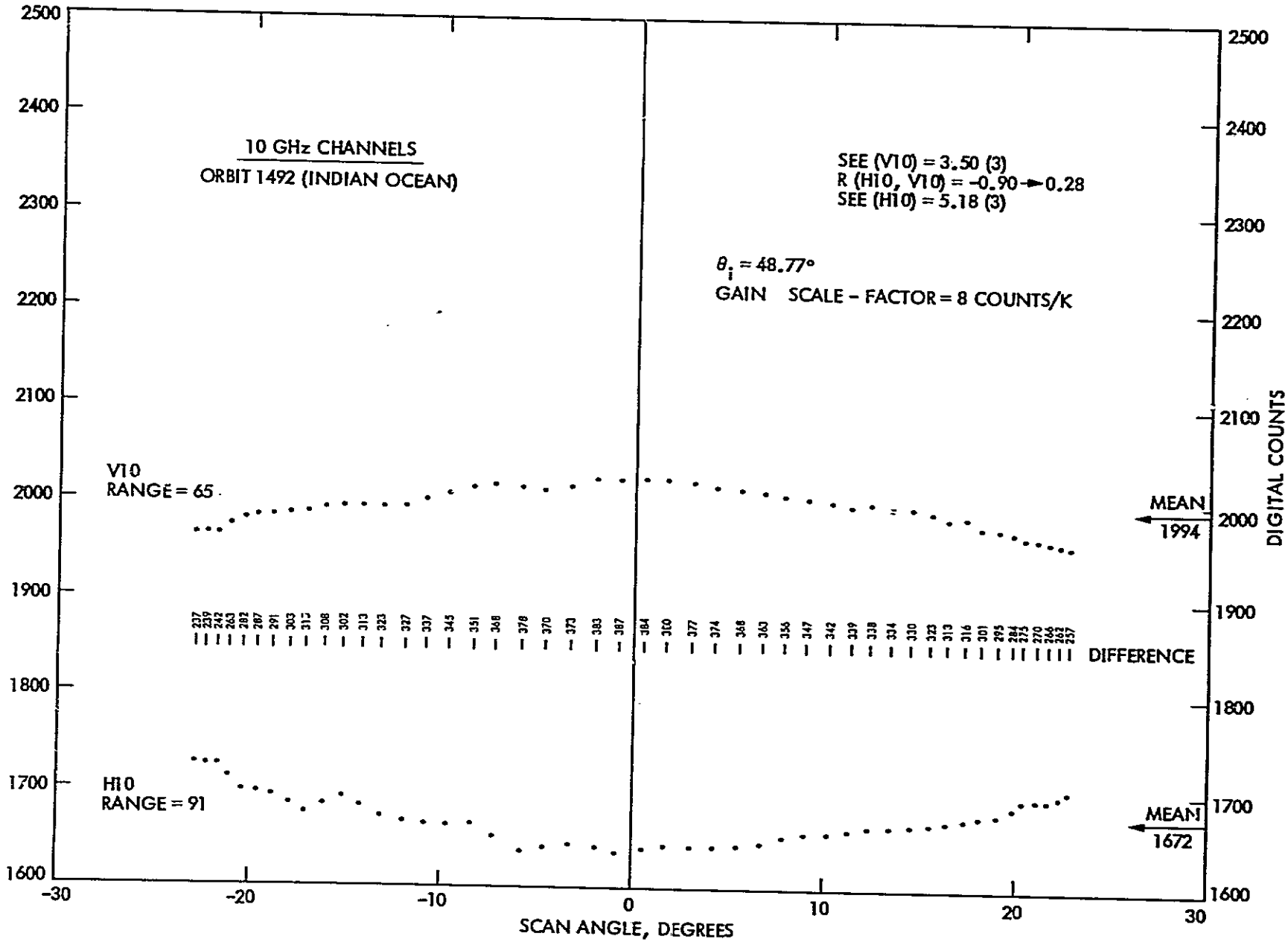

Figure E3-7. Indian Ocean 10-GHz Channels

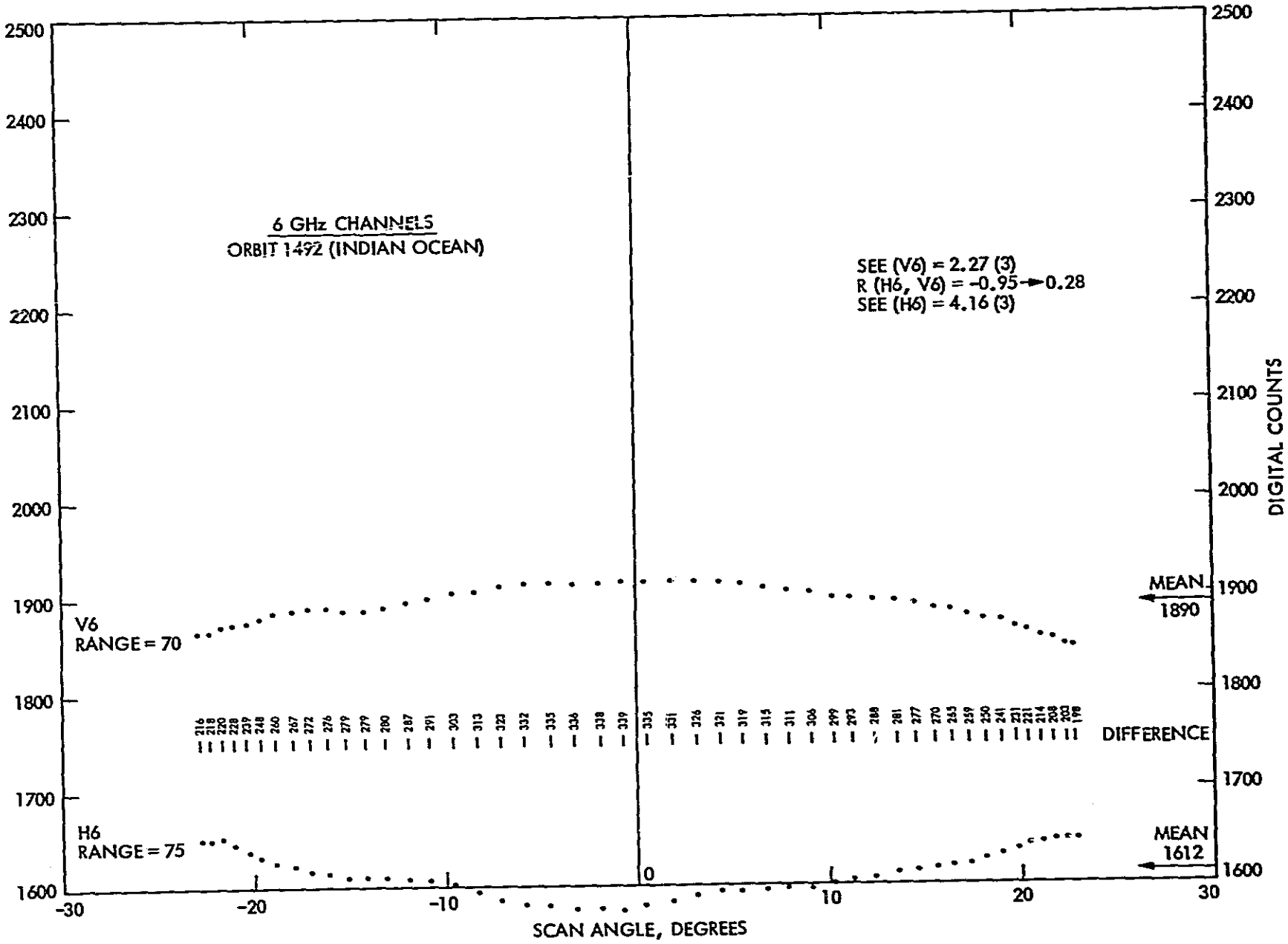

Figure E3-8. Indian Ocean 6-GHz Channels

EXHIBIT 4

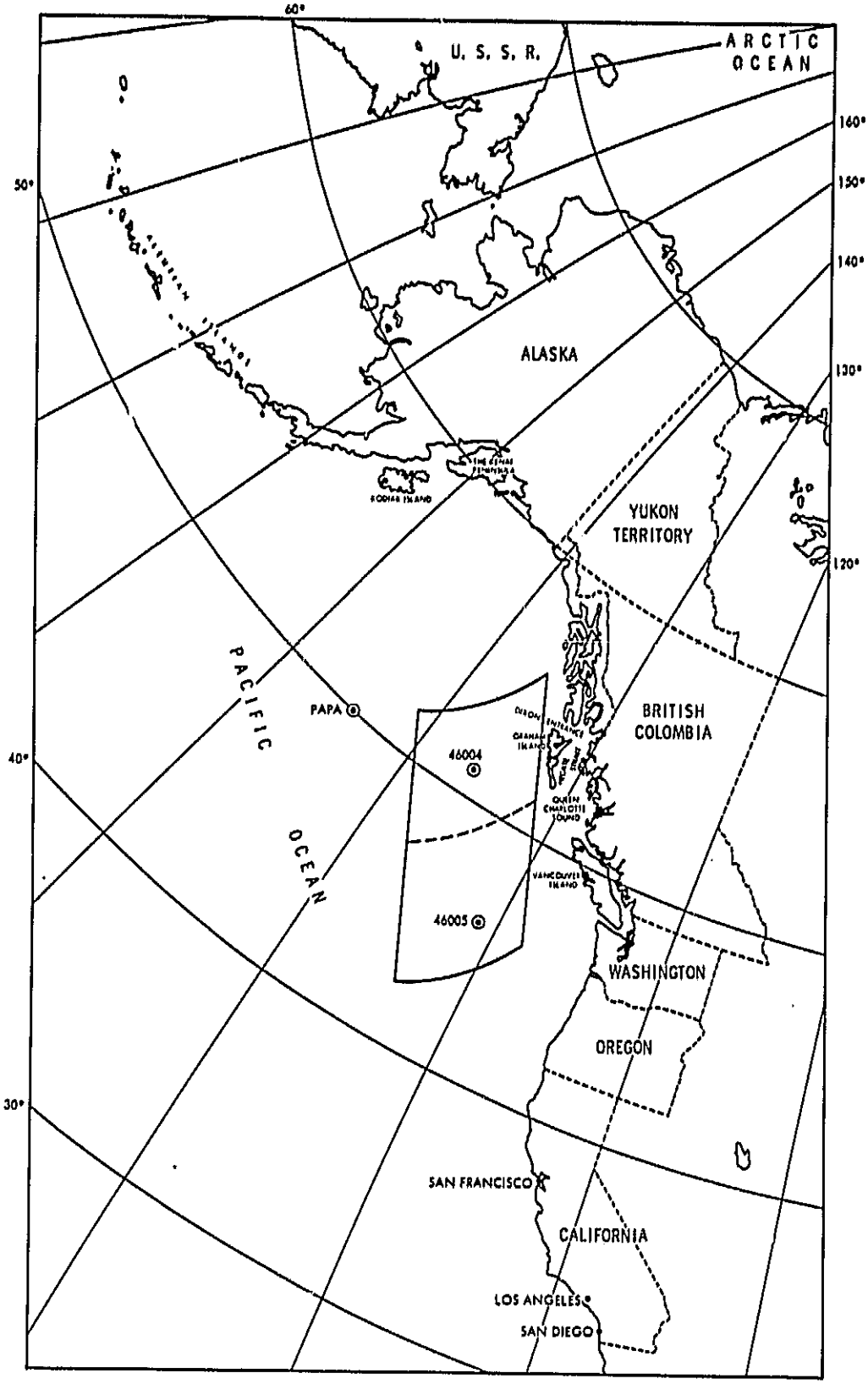

Figure E4-1. A Cloudy, Windy Sea - Near Land

Figure E4-2. An Infrared Image of the Cloudy, Windy Sea - Near Land. (The black ellipse appearing in the upper left quadrant is the center of the swath (scan angle = 0^{o}) as shown in dashed lines in Figure E4-1.)

Figure E4-3. A Visible Image of a Cloudy, Windy Sea - Near Land. (The white ellipse in the upper left quadrant is the center of the swath (scan angle = 0^{o}) as shown in dashed lines in Figure E4-1.)

Table E4-1. Wind and Sea States

WIND				
WIND FORCE	WIND EFFECTS	WIND SPEED (meters/sec)	WIND SPEED (s. miles/hour)	RELATIVE WIND (BEAUFORT SCALE)
CALM	SMOKE RISES VERTICALLY; NO PERCEPTIBLE MOVEMENT OF ANYTHING	< 0.45	< 1	0
LIGHT AIR	SMOKE DRIFT SHOWS WIND DIRECTION; BARELY MOVES TREE LEAVES	0.45 – 1.34	1 – 3	1
LIGHT BREEZE	WIND FELT ON FACE; LEAVES RUSTLE; SMALL TWIGS MOVE	1.79 – 3.13	4 – 7	2
GENTLE BREEZE	LEAVES AND TWIGS IN CONSTANT MOTION; BLOWS-UP DRY LEAVES FROM THE GROUND	3.58 – 5.36	8 – 12	3
MODERATE BREEZE	MOVES SMALL BRANCHES; RAISES DUST AND PAPER AND DRIVES THEM ALONG	5.81 – 8.05	13 – 18	4
FRESH BEEZE	LARGE BRANCHES AND SMALL TREES (IN LEAF) BEGIN TO SWAY; CRESTED WAVELETS FORM ON INLAND WATER	8.49 – 10.73	19 – 24	5
STRONG BREEZE	LARGE BRANCHES IN CONTINUOUS MOTION	11.18 – 13.85	25 – 31	6
MODERATE GALE	WHOLE TREES IN MOTION; INCONVENIENCE IN WALKING	14.3 – 16.99	32 – 38	7
FRESH GALE	BREAKS TWIGS AND SMALL BRANCHES; DIFFICULT TO WALK	17.43 – 20.56	39–46	8
STRONG GALE	LOOSENS BRICKS ON CHIMNEYS; BLOWS ROOFING SLATES OFF; LITTERS GROUND WITH BROKEN BRANCHES	21.01 – 24.14	47 – 54	9
WHOLE GALE	TREES UPROOTED; CONSIDERABLE STRUCTURAL DAMAGE	24.59 – 28.16	55 – 63	10
STORM	WIDE-SPREAD DAMAGE	28.61 – 33.53	64 – 75	11
HURRICANE	SEVERE AND EXTENSIVE DAMAGE	> 33.53	> 75	12

SEA-STATE	
SEA-STATE (RELATIVE SCALE)	WAVE HEIGHT (meters)
0	0
1	< 0.3
2	0.3 – 0.91
3	0.91 – 1.52
4	1.52 – 2.44
5	2.44 – 3.66
6	3.66 – 6.10
7	6.10 – 12.19
8	> 12.9
9	CONFUSED

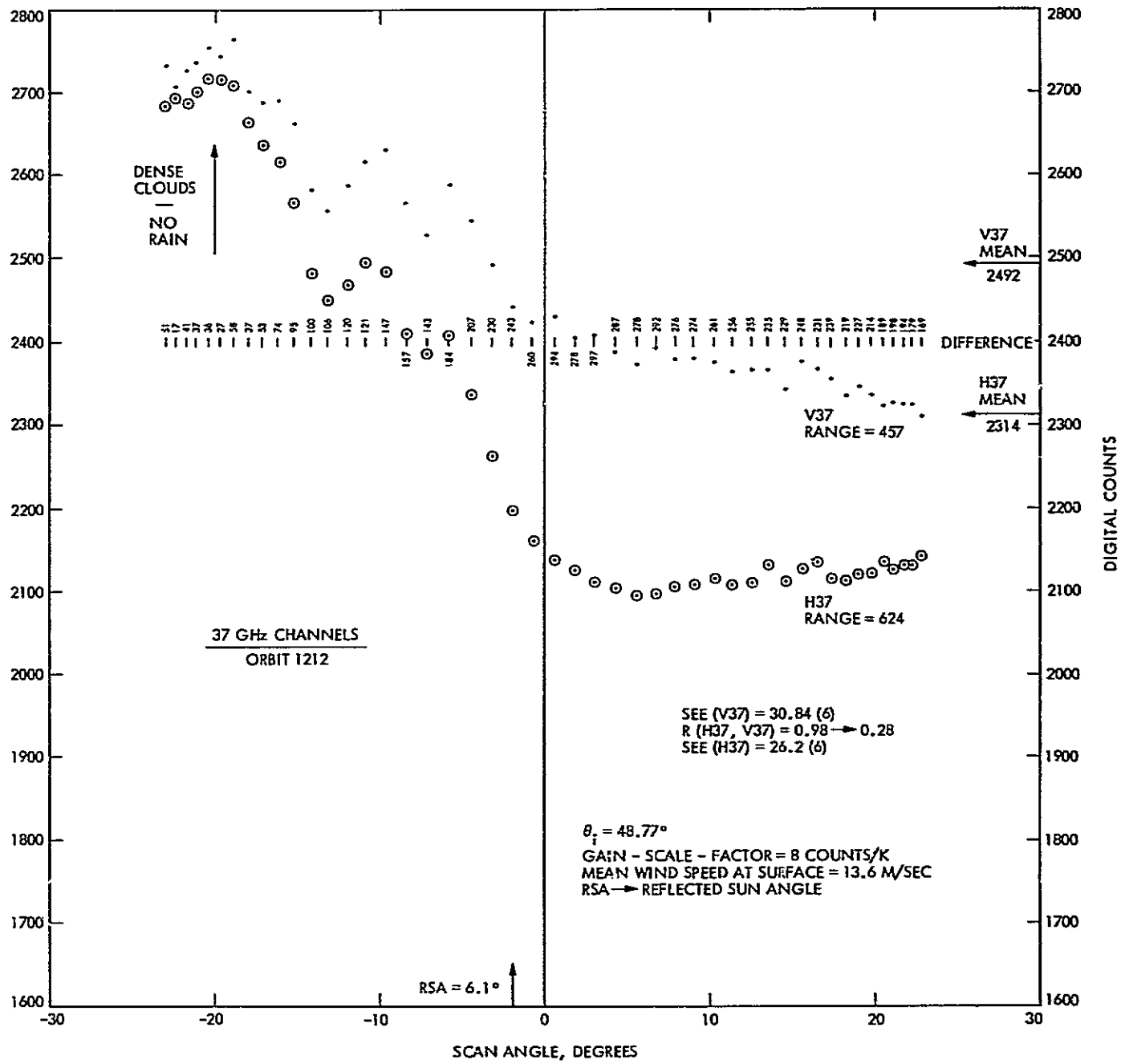

Figure E4-4. Channels at 37 GHz

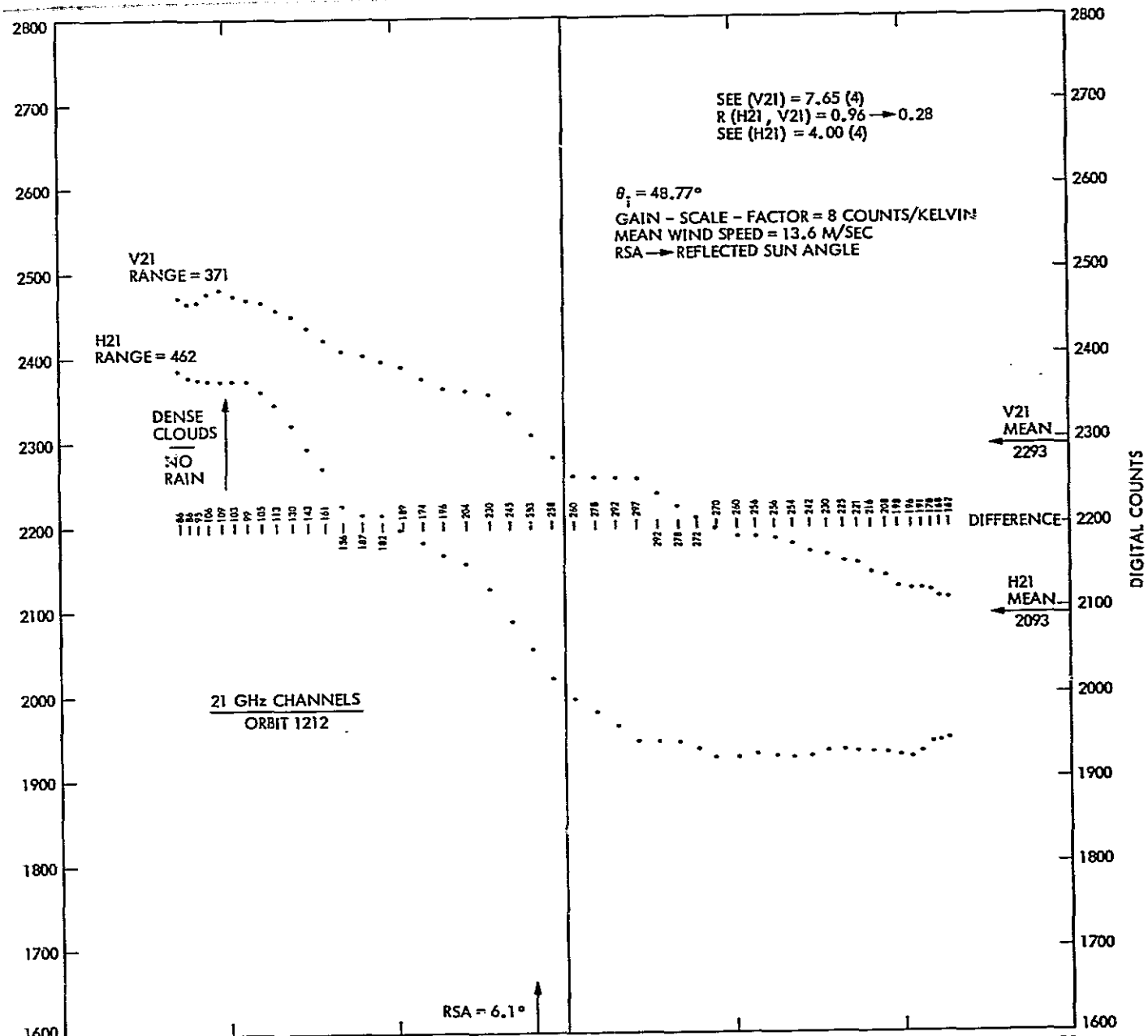

Figure E4-5. Channels at 21 GHz

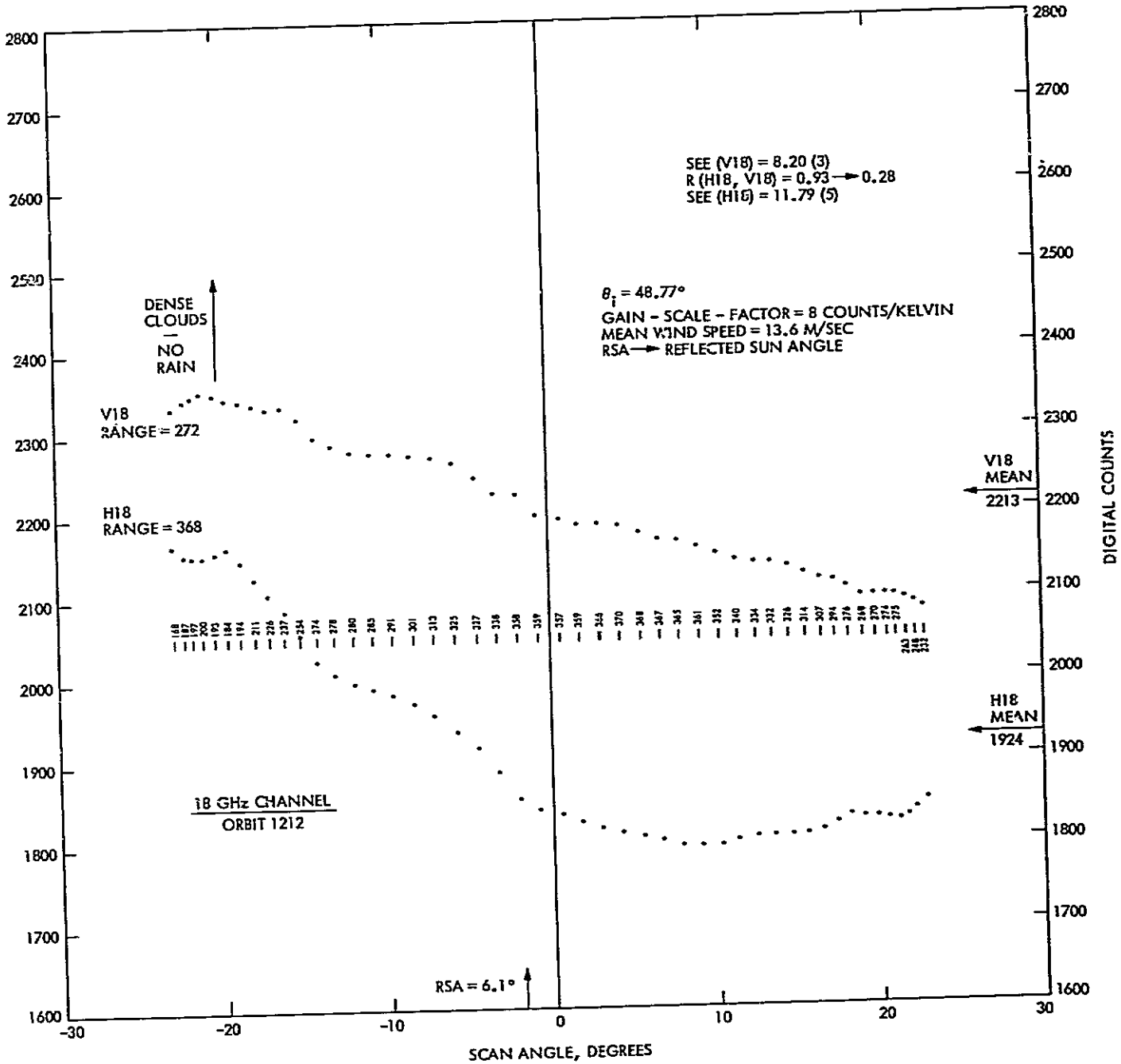

Figure E4-6. Channels at 18 GHz

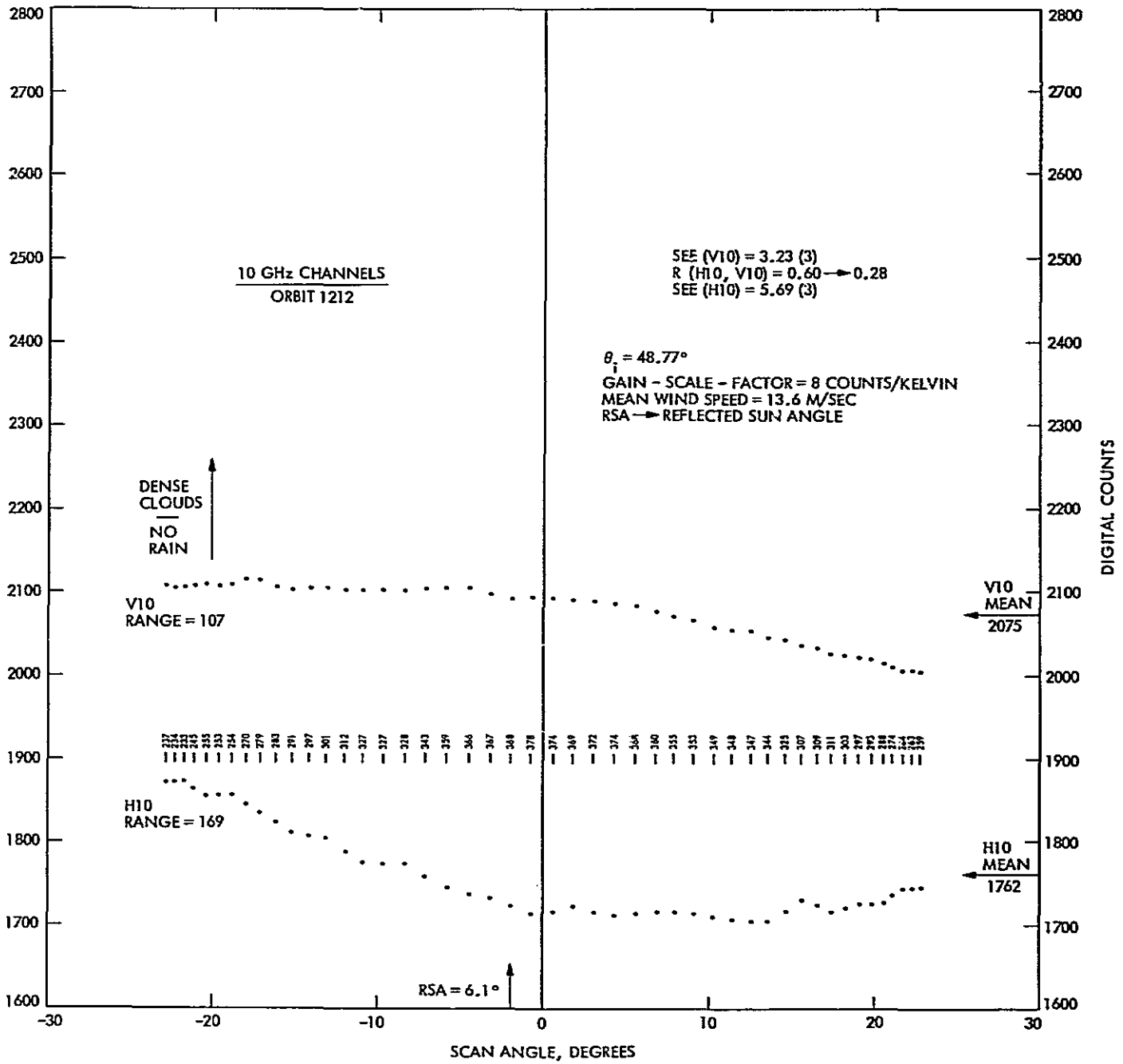

Figure E4-7. Channels at 10 GHz

ORIGINAL PAGE IS
OF POOR QUALITY

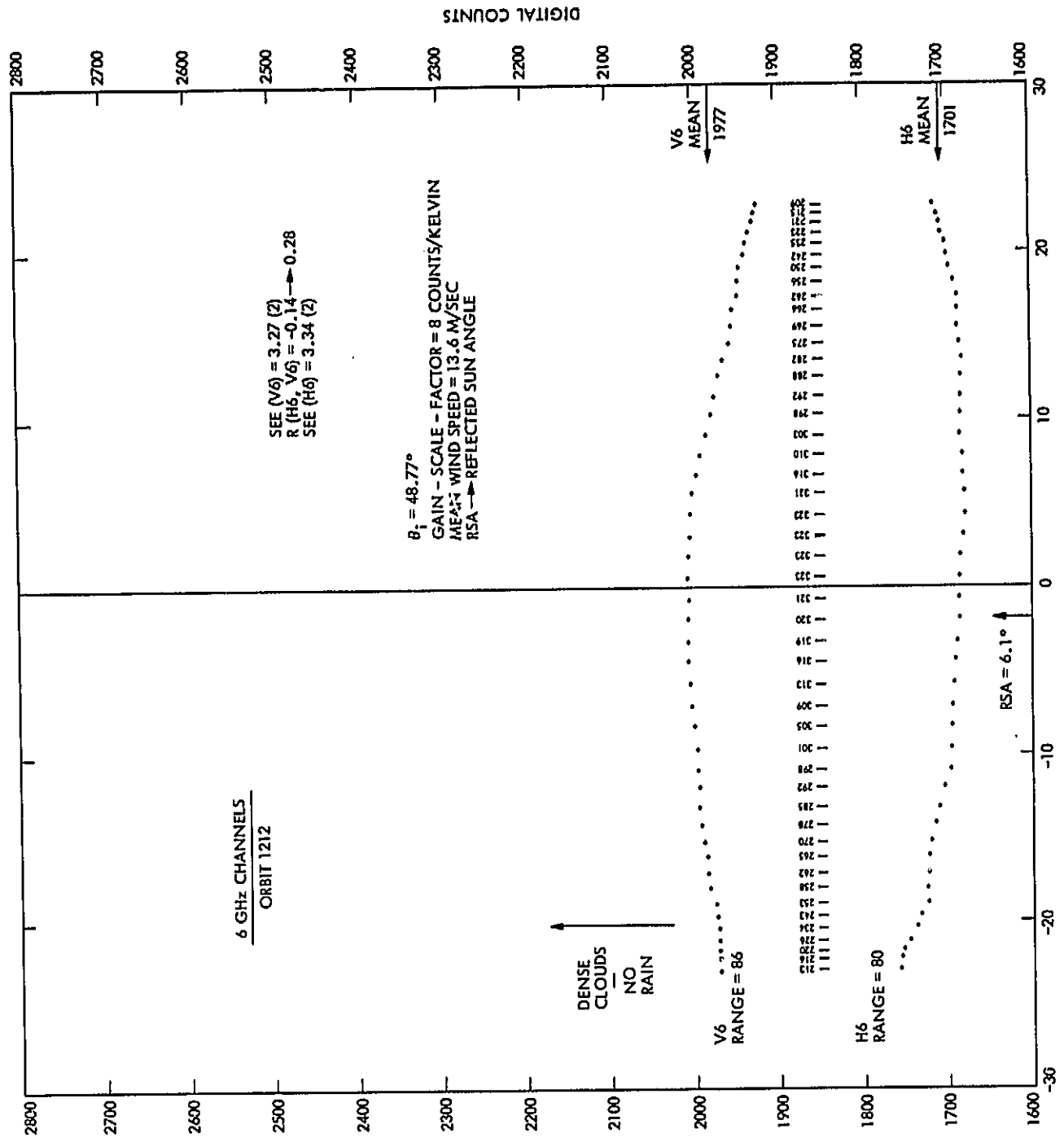

Figure E4-8. Channels at 6 GHz